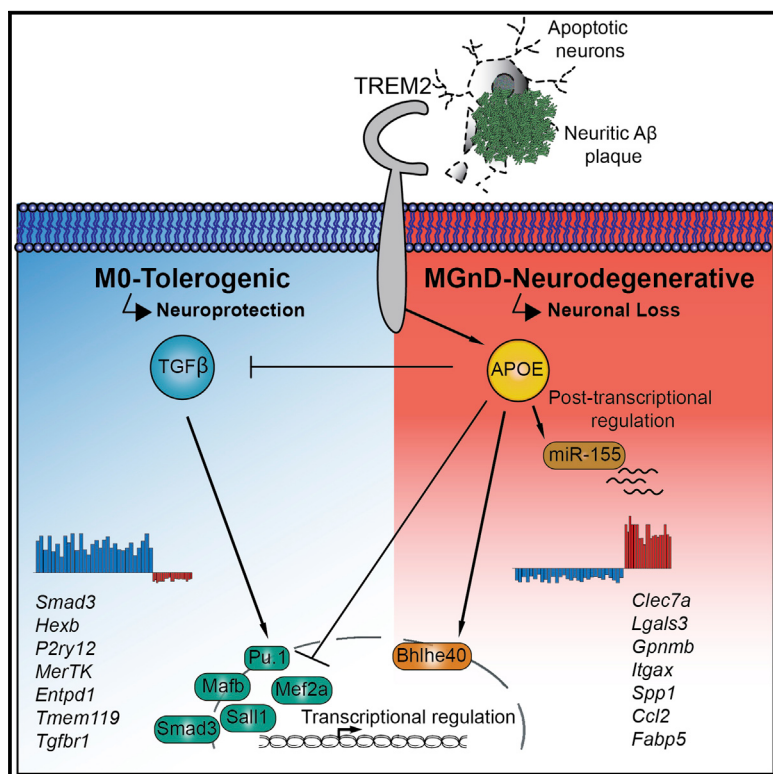


# The TREM2-APOE Pathway Drives the Transcriptional Phenotype of Dysfunctional Microglia in Neurodegenerative Diseases

## Graphical Abstract



## Authors

Susanne Krasemann,  
Charlotte Madore, Ron Cialic, ...,  
Jordi Ochando, Christian Haass,  
Oleg Butovsky

## Correspondence

[obutovsky@rics.bwh.harvard.edu](mailto:obutovsky@rics.bwh.harvard.edu)

## In Brief

Microglia change their phenotype and function during aging and neurodegeneration, but the underlying molecular mechanisms for this change remain unknown. Krasemann et al. identify the TREM2-APOE pathway as a major regulator of microglia phenotypic change in neurodegenerative diseases and suggest that targeting this pathway could restore homeostatic microglia.

## Highlights

- Microglia associated with neuritic A<sub>Beta</sub>-plaques exhibit a neurodegenerative phenotype
- Phagocytosis of apoptotic neurons suppresses homeostatic microglia
- The TREM2-APOE pathway regulates neurodegenerative microglial phenotypic switch
- Targeting APOE signaling restores homeostatic and tolerogenic microglia

# The TREM2-APOE Pathway Drives the Transcriptional Phenotype of Dysfunctional Microglia in Neurodegenerative Diseases

Susanne Krasemann,<sup>1,2,17</sup> Charlotte Madore,<sup>1,17</sup> Ron Cialic,<sup>1</sup> Caroline Baufeld,<sup>1</sup> Narghes Calcagno,<sup>1</sup> Rachid El Fatimy,<sup>1</sup> Lien Beckers,<sup>1</sup> Elaine O'Loughlin,<sup>1</sup> Yang Xu,<sup>3</sup> Zain Fanek,<sup>1</sup> David J. Greco,<sup>1</sup> Scott T. Smith,<sup>1</sup> George Tweet,<sup>1</sup> Zachary Humulock,<sup>1</sup> Tobias Zrzavy,<sup>4</sup> Patricia Conde-Sanroman,<sup>5</sup> Mar Gacias,<sup>5</sup> Zhiping Weng,<sup>6</sup> Hao Chen,<sup>6</sup> Emily Tjon,<sup>1</sup> Fargol Mazaheri,<sup>7</sup> Kristin Hartmann,<sup>2</sup> Asaf Madi,<sup>1</sup> Jason D. Ulrich,<sup>8</sup> Markus Glatzel,<sup>2</sup> Anna Worthmann,<sup>9</sup> Joerg Heeren,<sup>9</sup> Bogdan Budnik,<sup>10</sup> Cynthia Lemere,<sup>1</sup> Tsuneya Ikezu,<sup>11</sup> Frank L. Heppner,<sup>12,13</sup> Vladimir Litvak,<sup>3</sup> David M. Holtzman,<sup>8</sup> Hans Lassmann,<sup>4</sup> Howard L. Weiner,<sup>1,14</sup> Jordi Ochando,<sup>5</sup> Christian Haass,<sup>7,15,16</sup> and Oleg Butovsky,<sup>1,14,18,\*</sup>

<sup>1</sup>Ann Romney Center for Neurologic Diseases, Department of Neurology, Brigham and Women's Hospital, Harvard Medical School, Boston, MA, USA

<sup>2</sup>Institute of Neuropathology, University Medical Center Hamburg-Eppendorf, Hamburg, Germany

<sup>3</sup>Department of Microbiology and Physiological Systems, University of Massachusetts Medical School, Worcester, MA, USA

<sup>4</sup>Center for Brain Research, Medical University of Vienna, Vienna, Austria

<sup>5</sup>Department of Medicine, Icahn School of Medicine at Mount Sinai, NY, USA

<sup>6</sup>Department of Biochemistry and Molecular Pharmacology, University of Massachusetts Medical School, Worcester, MA, USA

<sup>7</sup>German Center for Neurodegenerative Diseases, Munich, Germany

<sup>8</sup>Department of Neurology, Hope Center for Neurological Disorders, Knight Alzheimer's Disease Research Center, Washington University School of Medicine, St. Louis, USA

<sup>9</sup>Department of Biochemistry and Molecular Cell Biology, University Medical Center Hamburg-Eppendorf, Hamburg, Germany

<sup>10</sup>Mass Spectrometry and Proteomics Resource Laboratory, Faculty of Arts and Sciences Division of Science, Harvard University, Cambridge MA, USA

<sup>11</sup>Department of Pharmacology and Experimental Therapeutics and Department of Neurology, Boston University School of Medicine, MA, USA

<sup>12</sup>Department of Neuropathology, Charité-Universitätsmedizin Berlin, Berlin, Germany

<sup>13</sup>Cluster of Excellence, NeuroCure, Charitéplatz 1, 10117 Berlin, Germany

<sup>14</sup>Evergrande Center for Immunologic Diseases, Brigham and Women's Hospital, Harvard Medical School, Boston, MA, USA

<sup>15</sup>Biomedical Center, Biochemistry, Ludwig-Maximilians-Universität Munich, Munich, Germany

<sup>16</sup>Munich Cluster for Systems Neurology, Munich, Germany

<sup>17</sup>These authors contributed equally

<sup>18</sup>Lead Contact

\*Correspondence: obutovsky@rics.bwh.harvard.edu

<http://dx.doi.org/10.1016/j.immuni.2017.08.008>

## SUMMARY

Microglia play a pivotal role in the maintenance of brain homeostasis but lose homeostatic function during neurodegenerative disorders. We identified a specific apolipoprotein E (APOE)-dependent molecular signature in microglia from models of **amyotrophic lateral sclerosis (ALS)**, **multiple sclerosis (MS)**, and **Alzheimer's disease (AD)** and in microglia surrounding neuritic β-amyloid (Aβ)-plaques in the brains of people with AD. The APOE pathway mediated a switch from a homeostatic to a neurodegenerative microglia phenotype after phagocytosis of apoptotic neurons. TREM2 (triggering receptor expressed on myeloid cells 2) induced APOE signaling, and targeting the TREM2-APOE pathway restored the homeostatic signature of microglia in ALS and AD mouse models and prevented neuronal loss in an acute model of neurodegeneration. APOE-mediated neurodegenerative microglia had lost their tolerogenic function. Our work identifies the TREM2-

APOE pathway as a major regulator of microglial functional phenotype in neurodegenerative diseases and serves as a novel target that could aid in the restoration of homeostatic microglia.

## INTRODUCTION

Neuronal injury and cell death are common hallmarks of neurodegenerative processes (Mattson, 2000). It remains unclear whether neuronal cell death is a cause or result of Alzheimer's disease (AD), especially when one considers that neurodegeneration is not an acute and rapid event but occurs gradually over a long period of time. However, apoptosis, as well as neuritic dystrophy leading to permanent central nervous system (CNS) damage, occurs in neurodegenerative diseases, including AD (Masliah et al., 1998) and amyotrophic lateral sclerosis (ALS) (Kostic et al., 1997), and in inflammatory autoimmune diseases such as multiple sclerosis (MS) (Ofengeim et al., 2015).

Microglia are brain-resident immune cells that maintain CNS homeostasis, constantly survey their environment (Nimmerjahn et al., 2005), and react to homeostasis-perturbing elements by

initiating an inflammatory reaction (Kreutzberg, 1996). In the healthy brain, they have a unique homeostatic molecular and functional signature (M0) (Butovsky et al., 2014; Gautier et al., 2012; Hickman et al., 2013), which is tightly controlled by transforming growth factor  $\beta$  (TGF $\beta$ ) signaling (Butovsky et al., 2014; Gosselin et al., 2014). However, during the course of disease, microglia lose their homeostatic molecular signature and functions (Butovsky et al., 2015; Holtzman et al., 2015) and become chronically inflammatory (Perry and Holmes, 2014). Recent studies identified a common disease-associated microglia signature (Chiu et al., 2013; Hickman et al., 2013; Holtzman et al., 2015; Keren-Shaul et al., 2017; Orre et al., 2014). However, the mechanisms that regulate the microglial phenotype in disease have not been identified.

In this study, we identified a role for apolipoprotein E (APOE) in regulating a subset of microglia, which exhibit a common disease-associated phenotype. This neurodegenerative phenotypic switch is triggered by TREM2, leading to activation of APOE signaling and subsequent suppression of homeostatic microglial phenotype. A functional consequence of the activation of TREM2-APOE pathway is that microglia lose the ability to regulate brain homeostasis.

## RESULTS

### Reciprocal Induction of APOE and Suppression of TGF $\beta$ Signaling in Disease-Associated Microglia

To investigate underlying common molecular mechanisms that regulate microglial dysfunction, we isolated microglia and analyzed transcriptomes during aging and disease progression in mouse models of ALS (SOD1<sup>G93A</sup>, expressing human Cu,Zn superoxide dismutase mutation), AD (APP-PS1, overexpressing mutated genes for human amyloid precursor protein and presenilin 1), and MS (experimental autoimmune encephalomyelitis [EAE]) (Table S1). We performed *k*-means clustering and identified two major gene clusters (Figure 1A). Cluster 1 was associated with the loss of 68 homeostatic microglial genes, including *P2ry12*, *Tmem119*, *Gpr34*, *Jun*, *Olfml3*, *Csf1r*, *Hexb*, *Mertk*, *Rhob*, *Cx3Cr1*, *Tgfb1*, and *Tgfb1* and transcription factors such as *Mef2a*, *Mafb*, *Jun*, *Sall1*, and *Egr1*, which are enriched in adult microglia (Butovsky et al., 2014; Buttgereit et al., 2016; Matcovitch-Natan et al., 2016). Cluster 2 was associated with the upregulation of 28 inflammatory molecules, including *Spp1*, *Itgax*, *Axl*, *Lilrb4*, *Clec7a*, *Ccl2*, *Csf1*, and *Apoe*, of which *Apoe* was one of the most upregulated genes (Figure 1A and Table S1). We termed this microglial neurodegenerative phenotype MGND, in contrast to M0-homeostatic adult microglia phenotype (Butovsky et al., 2014; Gautier et al., 2012; Hickman et al., 2013). Linear regression analysis showed a negative correlation of *Mef2a*, *Sall1*, and *Tgfb1* with progression in EAE, SOD1, and APP-PS1 models (Figure 1B). In contrast, induction of *Apoe* was positively correlated with progression (Figure 1B). In EAE, we found suppression of homeostatic genes (e.g., *P2ry12*, *Tmem119*, *Tgfb1*, *Mafb*, *Mef2a*, *Sall1*, and *Egr1*; Butovsky et al., 2014; Gautier et al., 2012; Hickman et al., 2013; Matcovitch-Natan et al., 2016) during the acute phase and restoration during recovery (Figure 1C; Figures S1A–S1C and Table S1). *Apoe* was reciprocally upregulated (Figure 1C), which we validated by quantitative real-time PCR (qPCR) in two other

MOG-induced EAE mouse models: the non-obese diabetic (NOD) (chronic-relapsing) model and the C57BL/6J (acute) model (Figures S1D and S1E). *P2ry12* immunoreactivity was lost at onset and disease peak and re-emerged during recovery (Figure S1F). *Apoe* and *TGF $\beta$*  were major upstream regulators of MGND microglia (Figure 1D and Table S1), as shown by ingenuity pathway analysis (IPA). The top-suppressed TGF $\beta$ -dependent homeostatic genes (Butovsky et al., 2014), *Olfml3*, *P2ry12*, *Tmem119*, *Mef2a*, *Jun*, *Sall1*, and upregulated genes *Apoe* and *Axl* were similarly affected during progression (Figure 1E). These results indicate a common disease-related microglia molecular signature that is associated with the induction of *Apoe* and the suppression of TGF $\beta$  signaling.

### The MGND-Microglia Subset Is Associated with Neuritic A $\beta$ Plaques and Diffuse Neuritic Dystrophy in the AD Cortex

The pathology of the AD brain is characterized by widespread neuritic dystrophy (Larner, 1995). These dystrophic axons are enlarged and show intense reactivity for phosphorylated neurofilaments (Sternberger et al., 1985). To address whether a microglial phenotypic switch from M0 homeostatic to MGND-neurodegenerative is specifically associated with neuritic dystrophy in AD, we analyzed brains from APP-PS1 mice and humans with AD. To distinguish M0 versus MGND microglia, we used *P2ry12* and *Clec7a* mAbs and found *Clec7a*<sup>+</sup>*P2ry12*<sup>−</sup> microglia associated with A $\beta$  plaques in APP-PS1 mice (Figure 2A). We identified three microglial subsets: (1) *Clec7a*<sup>−</sup>*P2ry12*<sup>+</sup> (not associated with A $\beta$  plaques); (2) *Clec7a*<sup>lo</sup>*P2ry12*<sup>lo</sup> (in close proximity to A $\beta$  plaques); and (3) *Clec7a*<sup>+</sup>*P2ry12*<sup>−</sup> (associated with neuritic A $\beta$  plaques) (Figure 2A). *Tmem119* is stable even when the mRNA is downregulated (Satoh et al., 2016) and co-localized with A $\beta$ -plaque-associated *Clec7a*<sup>+</sup> microglia (Figure S2A). *Clec7a*<sup>+</sup>*P2ry12*<sup>−</sup> microglia were associated with phosphorylated neurofilaments (pNF $^+$ ) in neuritic plaques in APP-PS1 mice (Figure 2B and Figure S2B). The number of FCRLS<sup>+</sup>*Clec7a*<sup>+</sup> microglia was increased in 24-month-old APP-PS1 mice (Figures S2C–S2G). The phenotype of *Clec7a*<sup>+</sup> microglia was similar to that of MGND microglia identified in SOD1, EAE, and APP-PS1 models and during aging (Figure 2C and Table S2). Suppressed microglial homeostatic genes included *P2ry12*, *Tmem119*, *Olfml3*, *Csf1r*, *Rhob*, *Cx3cr1*, *Tgfb1*, *Mef2a*, *Mafb*, and *Sall1*, and upregulated inflammatory molecules included *Spp1*, *Itgax*, *Axl*, *Lilrb4*, *Clec7a*, *Csf1*, and *Apoe*, the latter of which was among the most upregulated genes (Figures 2C and 2D and Table S2). Transition from *Clec7a*<sup>−</sup> to *Clec7a*<sup>int</sup> to *Clec7a*<sup>hi</sup> correlated with increased expression of *Apoe* and suppression of homeostatic molecules (Figure 2D). *Clec7a* expression increased during progression in EAE and SOD1 mice (Figures S2H–S2K). RNA sequencing (RNAseq) of the three microglia subsets validated the NanoString analysis and showed that only FCRLS<sup>+</sup>*Clec7a*<sup>+</sup> microglia acquired an MGND signature (Figures 2E and 2F and Table S2).

To determine whether a microglial phenotype was associated with neuritic plaques, we double stained brains of individuals affected by AD for P2RY12 with A $\beta$  or pNF. P2RY12<sup>+</sup> microglia were preserved in A $\beta$  diffuse plaques, and P2RY12 signal was lost in pNF $^+$  neuritic plaques (Figure 2G). *TMEM119*<sup>+</sup>*P2RY12*<sup>−</sup> microglia, and not recruited IBA1<sup>+</sup>*TMEM119*<sup>−</sup> peripheral

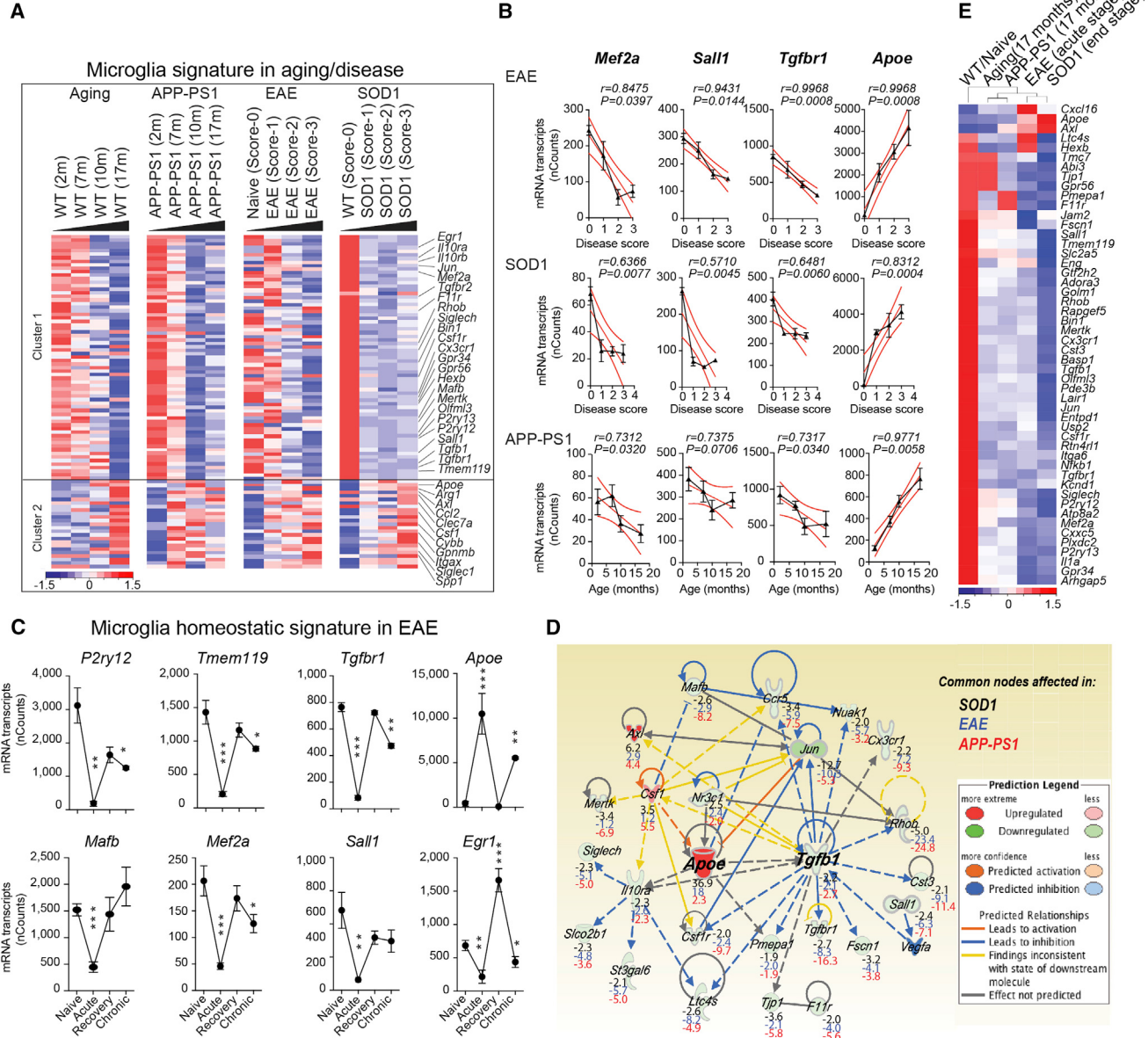


**Figure 1. Reciprocal Induction of APOE and Suppression of TGF $\beta$  Signaling in Disease-Associated MGND-Microglia**

(A) K-means clustering, via NanoString, of 95 significantly affected common genes in FCRLs $^+$  microglia during aging and disease. Vertical lanes are biological replicates per disease stage or condition in WT aging ( $n = 12$ ), EAE ( $n = 18$ ), SOD1 ( $n = 11$ ) and APP-PS1 ( $n = 12$ ) mice. Cluster 1: suppressed homeostatic genes. Cluster 2: upregulated genes.

(B) Linear regression curve of *Mef2a*, *Sall1*, *Tgfb1r*, and *Apoe* in EAE ( $n = 4\text{--}6$  mice/disease score) and SOD1 ( $n = 2\text{--}4$  mice/disease score) spinal-cord microglia and APP-PS1 ( $n = 3$  mice/age) brain microglia. Thick line: 95% confidence interval of the regression line.

(C) Selected homeostatic and disease-associated microglial genes during EAE ( $n = 3$ ). Data are presented as means  $\pm$  SEM. \* $p < 0.05$ , \*\* $p < 0.01$ , \*\*\* $p < 0.001$  by one-way ANOVA followed by Dunnett's multiple-comparison post-hoc test.

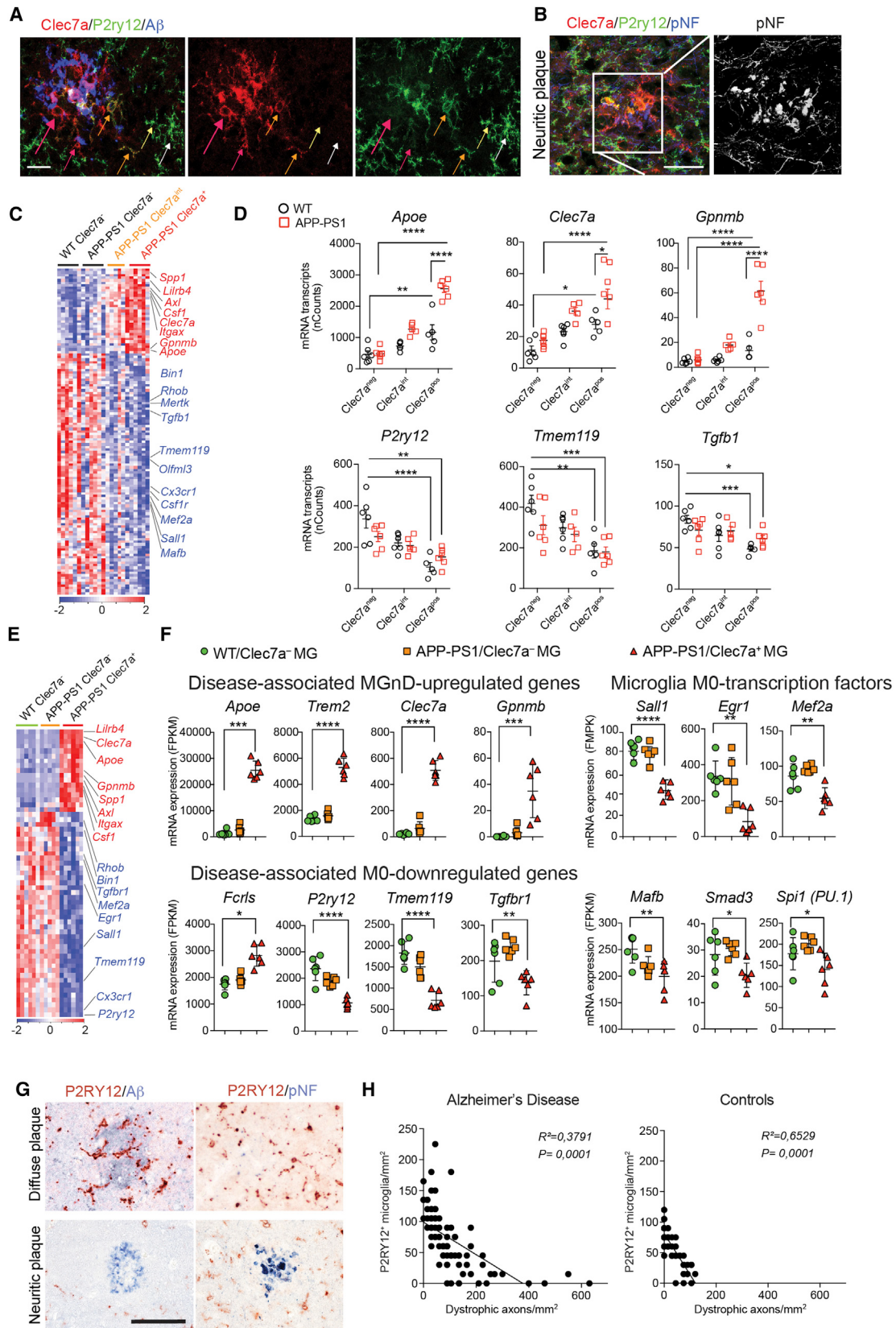
(D) IPA shows common nodes significantly affected in microglia in all three-mouse models in disease. For each molecule, the expression fold change compared to normal, homeostatic microglia is presented.

(E) Heatmap of significantly affected genes dysregulated in all 3 diseases ( $n = 3\text{--}4$ ) determined by NanoString. Vertical lanes: mean of biological replicates per disease stage/condition as indicated in (A).

See also Figure S1 and Table S1.

myeloid cells, were associated with pNF $^+$  neuritic plaques (Figures S2L–S2N). Loss of P2RY12 $^+$  microglia correlated with axonal dystrophy, but not with the extent of A $\beta$  deposition (Fig-

ure 2H). We found increased APOE expression in microglia in close proximity to A $\beta$  plaques (Figures S2O and S2P). These data demonstrate that the microglial phenotypic switch from



(legend on next page)

M0 to MGnD is associated with neuritic dystrophy in APP-PS1 mice and AD-affected humans.

### Phagocytosis of Apoptotic Neurons Suppresses Homeostatic Microglia

To determine the mechanisms by which the MGnD microglia are induced in neurodegeneration, we injected apoptotic neurons (dNs) into the cortex and hippocampus of naive mice. dNs induced the recruitment of P2ry12<sup>+</sup> microglia toward the site of injection (Figure 3A). P2ry12<sup>+</sup> microglia changed morphology from an M0 homeostatic non-phagocytic (MG-nΦ) phenotype to an amoeboid-phagocytic (MG-dNΦ) phenotype at the vicinity of the injection site (Figures 3A–3C and Figure S3A). Induction of MGnD microglia was not detected in phosphate-buffered saline (PBS)-injected brains (Figure S3B). Apoptotic neurons were internalized by P2ry12<sup>+</sup> microglia (Figure 3B). Induction of Apoe was detected in MG-dNΦ microglia (Figure 3C). Increased Apoe expression was detected as early as 3 hr after injection and peaked at 16 hr after injection (Figure S3C). Restoration of homeostatic P2ry12<sup>+</sup>Clec7a<sup>-</sup> microglia occurred at 14 d post-injection (Figures S2D and S2E). Profiling of MG-dNΦ and MG-nΦ microglia showed that phagocytosis of dNs induced a microglial molecular phenotype similar to the MGnD phenotype (Figures 3D and 3E). M0-microglial homeostatic genes including *Tmem119*, *Egr1*, *Hexb*, *Gpr34*, *P2ry12*, *Olfml3*, and *Tgfb1* were suppressed in MG-dNΦ microglia, whereas *Apoe* was the major upregulated gene among other inflammatory molecules (Figure 3F and Table S3). This was confirmed by qPCR of microglial genes including upregulation of *Apoe* and microRNA miR-155 (Figure 3G and Figures S3C and S3F). Although injured neurons express elevated *Apoe* (Xu et al., 2006), we observed the upregulation of *Apoe* in MG-dNΦ microglia phagocytosing *Apoe*<sup>-/-</sup> dNs (Figure S3G). Injection of *E. coli* or zymosan particles did not induce *Apoe* in phagocytic microglia (Figure S3H). In contrast, miR-155 was induced by dNs, *E. coli* and zymosan particles in phagocytic microglia (Figure S3I). Microglia phagocytosed injected dNs, but not live neurons (Figures S3J and S3K). Upregulation of *Apoe* in phagocytic microglia was also induced by apoptotic monocytes (Figure S3L). We validated our paradigm of dN-induced MG-dNΦ phenotype by using kainic acid as a model of acute neuronal cell death (Lévesque and Avoli, 2013). We observed P2ry12<sup>+</sup>Clec7a<sup>+</sup> microglia 48 hr post-injection (Figure S4).

Although in vivo LPS and IFN-γ-stimulated microglia suppressed many of the homeostatic microglial genes including *P2ry12*, *Gpr34*, *Fcrls*, *Tmem119*, *Olfml3*, *Siglech*, *Sall1*, *Hexb*, *Csf1r*, and *Tgfb1* (Figures S5A–S5C and Table S4), the expression of *Apoe* was suppressed in M1 microglia (Figures S5D–S5E and S5H). In contrast, *Egr1*, which is a key transcription factor in M0 homeostatic microglia (Butovsky et al., 2014; Matcovitch-Natan et al., 2016) and was most suppressed in MG-dNΦ microglia, was induced in M1 microglia (Figures S5F–S5H). Furthermore, arginase 1 (*Arg1*) and chitinase-3-like protein (*Ym1*), the “classical” M2 anti-inflammatory markers, (Martinez and Gordon, 2014) were induced in MG-dNΦ microglia along with inflammatory molecules, including those encoded by *Il1b*, *Ptgs2* (*Cox2*), *Ccl2*, *Ccl5*, *Tspo*, *Msr1*, and *Cebpb* (Figures S5F–S5H). Thus, the MG-dNΦ molecular signature is distinct from that of classical M1induced microglia.

Quantitative mass spectrometry of MG-dNΦ versus MG-nΦ microglia showed increased amounts of *Apoe* and *Lgals3* in MG-dNΦ microglia. In contrast, both *Rgs10* and *Bin1*, two homeostatic microglial proteins (Butovsky et al., 2014), were suppressed (Figure 3H and Table S3). To investigate MG-dNΦ microglia in disease models, we used gene-set enrichment analysis (GSEA). Circos plot network analysis presented an overlap of the phagocytic microglial phenotype with the microglia molecular signature during aging and in a model of brain irradiation. The MG-dNΦ microglia signature was enriched in microglia transcriptomes from models of AD (5XFAD), ALS (SOD1), and *Mcp2* deficiency, which is associated with cerebellar degeneration (Verheijden et al., 2013). In contrast, microglial changes in *Mcp2* deficiency, or changes associated with neuropathic and chronic pain models were not connected with the MG-dNΦ gene signature (Figure 3I and Table S3). Taken together, these data show that MGnD microglia are induced by apoptotic neurons, which are a hallmark of neurodegeneration.

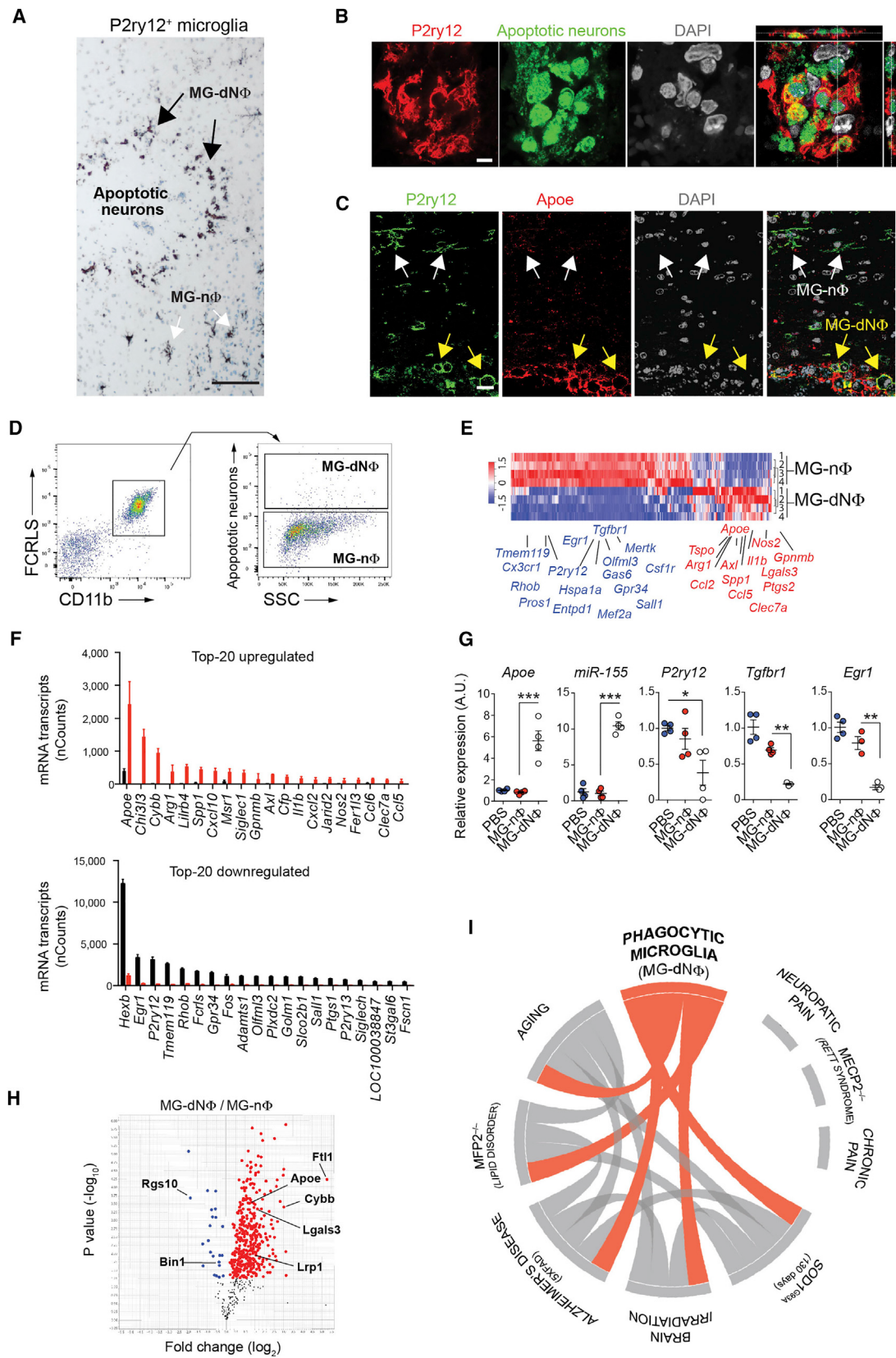
### APOE Regulates the Transcriptional and Post-transcriptional Program of the MGnD Phenotype and Function

We previously reported that *Apoe* expression is downregulated in microglia during development, correlates with the induction of M0-homeostatic genes, and is increased in microglia progenitors from CNS *Tgfb1*<sup>-/-</sup> mice (Butovsky et al., 2014). To assess the role of *Apoe* in the induction of MGnD microglia during

#### Figure 2. MGnD-Microglia Are Associated with Neuritic Aβ-Plaques

- (A) Staining for P2ry12<sup>+</sup> and Clec7a<sup>+</sup> in Aβ-plaque microglia in 24-month-old APP-PS1 mice. MGnD around plaque (red arrows). MGnD transitioning to plaque (yellow arrows). M0 homeostatic microglia (white arrows). Scale bar, 20 μm.
- (B) Staining for P2ry12<sup>+</sup> and Clec7a<sup>+</sup> in microglia associated with neuritic plaque (pNF) in 24-month-old APP-PS1 mice. Scale bar, 20 μm.
- (C) Heatmap of significantly affected genes in Clec7a<sup>+</sup> versus Clec7a<sup>int</sup> versus Clec7a<sup>-</sup> FCRLS<sup>+</sup> microglia in APP-PS1 versus WT mice (n = 5; 24 month). Selected homeostatic (blue) and inflammatory (red) genes.
- (D) Selected genes shown in (C). Dot plots: mRNA transcripts (mean ± SEM). \*p < 0.05, \*\*p < 0.01, \*\*\*p < 0.001, \*\*\*\*p < 0.0001 by one-way ANOVA followed by Tukey's multiple-comparison post-hoc test.
- (E) Heatmap of significantly affected genes determined by RNaseq in Clec7a<sup>+</sup> versus Clec7a<sup>-</sup> FCRLS<sup>+</sup> microglia in APP-PS1 versus WT mice (n = 5; 9 month).
- (F) Selected genes shown in (E). Dot plots: FPKM (mean ± s.e.m.). \*p < 0.05, \*\*p < 0.01, \*\*\*p < 0.001, \*\*\*\*p < 0.0001 by one-way ANOVA followed by Tukey's multiple-comparison post hoc test.
- (G) Staining for P2RY12 with Aβ or pNF in diffuse versus neuritic plaques in human AD brain. Scale bar, 100 μm.
- (H) Linear regression curve of P2RY12<sup>+</sup> microglia with dystrophic axons in temporal cortex of individuals (n = 14) with AD, as defined by CERAD criteria and Braak stages, and in temporal cortex from age-matched controls (n = 10).

See also Figure S2 and Table S2.



(legend on next page)

phagocytosis of neurons, we analyzed *Apoe*<sup>-/-</sup> versus WT transcriptomes from MG-nΦ versus MG-dNΦ microglia. We defined clusters on the basis of genes that were differentially expressed in WT non-phagocytic versus phagocytic versus *Apoe*<sup>-/-</sup> phagocytic microglia (Figure 4A and Table S5). Cluster 1 showed 885 genes that were induced in MG-dNΦ WT microglia but that were repressed in *Apoe*<sup>-/-</sup> MG-dNΦ microglia. 17 genes among those commonly upregulated in disease (Figure 1A) were suppressed by *Apoe* (Figure 4A and Table S5); such genes included *Clec7a*, *Gpnmb*, and *Lgals3* (Figure 4B) as well as *Bhlhe40* and others encoding transcription factors (TFs) commonly induced in disease (Figure 4C). Clusters 2 and 3 showed 1,220 genes that were suppressed in WT MG-dNΦ but that were restored in *Apoe*<sup>-/-</sup> MG-dNΦ microglia. Among 68 genes commonly suppressed in disease, 40 genes, including the major homeostatic genes *Tmem119*, *Tgfb1r*, and *Csf1r* (Figure 4D) and TFs such as *Mef2a*, *Mafb*, and *Sall1* (Figure 4E), were restored in *Apoe*<sup>-/-</sup> phagocytic microglia. NanoString confirmed de-repression of major homeostatic microglial genes (Figure S6A and Table S5). Disease-associated upregulated genes including *Lgals3* and *Clec7a* were suppressed in *Apoe*<sup>-/-</sup> microglia (Figure S6B). To assess the possibility of an intrinsic role of APOE regulation in a cell-specific manner, we deleted *Apoe* in microglia from *Cx3cr1*<sup>CreERT2</sup>:*Apoe*<sup>f/f</sup> mice. qPCR analysis confirmed *Apoe* deletion in *Cx3cr1*<sup>CreERT2</sup>:*Apoe*<sup>f/f</sup> microglia as compared to *Cx3cr1*<sup>WT</sup>:*Apoe*<sup>f/f</sup> microglia. Moreover, gene expression of *Clec7a* was repressed, and expression of *Csf1r*, *Tgfb1r*, and *Tmem119* was restored in MG-dNΦ microglia from *Cx3cr1*<sup>CreERT2</sup>:*Apoe*<sup>f/f</sup> mice (Figure 4F). Intrinsic deletion of *Apoe* did not affect expression of these genes in MG-nΦ microglia (Figure 4G), demonstrating that *Apoe* deletion had no effect on non-phagocytosing microglia.

A recent report showed induction of *Apoe* among other disease-associated genes in microglia 7 days after facial nerve axotomy (Tay et al., 2017). We assessed the role of *Apoe* on neuronal survival in WT, *Apoe*<sup>-/-</sup>, *Cx3cr1*<sup>CreERT2</sup>:*Apoe*<sup>f/f</sup>, and control *Cx3cr1*<sup>WT</sup>:*Apoe*<sup>f/f</sup> mice. Global and conditional deletion of *Apoe* in microglia reduced neuronal loss in *Cx3cr1*<sup>CreERT2</sup>:*Apoe*<sup>f/f</sup> mice as compared to WT or *Cx3cr1*<sup>WT</sup>:*Apoe*<sup>f/f</sup> mice in the axotomized facial motor nucleus (Figures 4H–I and Figure S6C). These data demonstrated the essential role of microglial *Apoe* in the MGnD phenotype.

Genetic ablation of miR-155 reverses the abnormal microglial signature and ameliorates disease in SOD1 mice (Butovsky et al., 2015). In MG-dNΦ microglia from *Apoe*<sup>-/-</sup> mice, miR-155 expression was suppressed (Figure S6D). In contrast, expression of *Apoe* was unaffected in miR-155<sup>-/-</sup> MG-dNΦ microglia (Figure S6E). Thus, miR-155 expression was regulated downstream of the APOE pathway. IPA upstream-regulator analysis identified TGFβ1 as the most significantly de-repressed molecule in *Apoe*<sup>-/-</sup> phagocytic microglia (Figure S6F). The top upstream regulator in miR-155<sup>-/-</sup> phagocytic microglia was IL-6 (Figure S6F), suggesting that its role in regulation of MGnD microglia was different from that of other proteins involved in inflammatory signaling. The *Egr1* transcription factor was the most de-repressed gene in the TGFβ pathway in *Apoe*<sup>-/-</sup> phagocytic microglia (Figure S6F). We determined the *Apoe*-dependent transcriptional effect in microglia by injecting recombinant *Apoe* intra-hippocampally in *Apoe*<sup>-/-</sup> mice. MGnD disease-associated genes such as *Msr1*, *Lirb4*, and *Tlr2* were induced, and homeostatic transcriptional factors including *Smad3*, *Mef2a*, *Mafb*, and *Egr1* were suppressed (Figures S6G and S6H and Table S5). Thus, APOE signaling has a twofold effect on microglia regulation in neurodegeneration: (1) suppression of the microglial homeostatic transcriptional factors, including *Mef2a*, *Mafb*, and *Smad3*, and (2) induction of an inflammatory program involving transcription factors *Bhlhe40*, *Tfec*, and *Atf3*, and a transcriptional and translational regulator, miR-155.

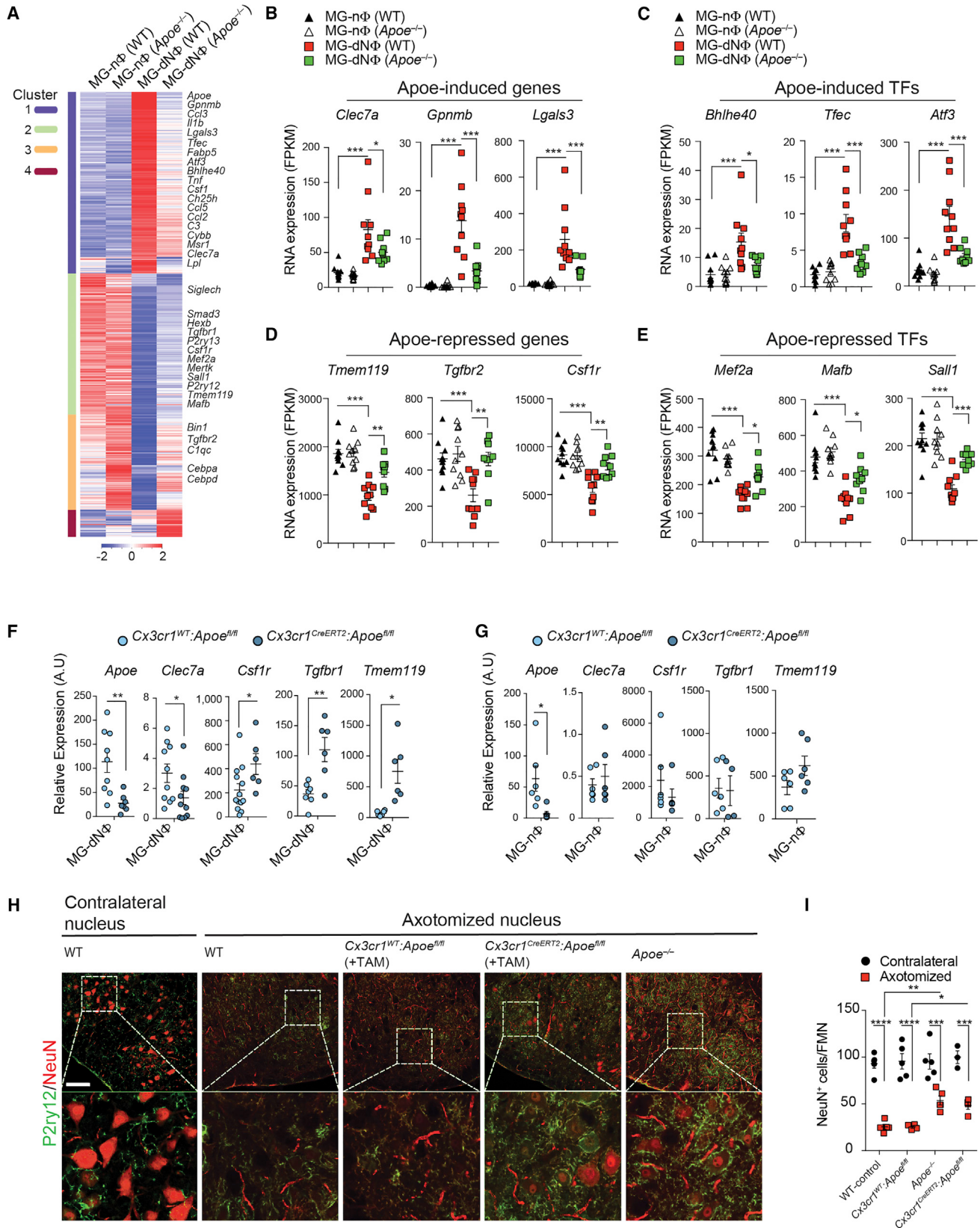
### Genetic Targeting of *Trem2* Suppresses the APOE Pathway and Restores the Homeostatic Microglia in APP-PS1 and SOD1 Mice

*TREM2* is a sensor of membrane-associated lipids, including phosphatidylserine (PS), which is focally exposed on apoptotic cells and processes or synapses of damaged neurons (Wang et al., 2015). We found that blocking phosphatidylserine on dNs with Annexin V (Koopman et al., 1994) reduced microglial phagocytosis by 88% (Figure S7A). Because dNs suppressed homeostatic microglia genes, we asked whether they activated the APOE pathway in a TREM2-dependent manner. We found that expression of homeostatic genes, including *P2ry12*, *Gpr34*, *Tmem119*, *Tgfb1r*, and *Csf1r* was restored to WT levels in *Trem2*<sup>-/-</sup> MG-dNΦ microglia (Figure 5A), whereas *Apoe* and

### Figure 3. Phagocytosis of Apoptotic Neurons Suppresses Homeostatic Microglia

For a Figure360 author presentation of Figure 3, see <http://dx.doi.org/10.1016/j.jimmuni.2017.08.008#mmc8>.

- (A) Staining for P2ry12<sup>+</sup> microglia at the site of apoptotic-neuron injection 16 hr after injection in WT mice (n = 6). Phagocytic (MG-dNΦ) and non-phagocytic (MG-nΦ) microglia. Scale bar, 80 μm.
  - (B) Orthogonal projections of confocal z stacks show intracellular Alexa488<sup>+</sup> dNs co-stained with DAPI in P2ry12<sup>+</sup> microglia (n = 6). Scale bar, 5 μm. One of two individual experiments.
  - (C) Staining for *Apoe* in P2ry12<sup>+</sup> MG-dNΦ. White arrows: *Apoe*<sup>-</sup> MG-nΦ; yellow arrows: *Apoe*<sup>+</sup> MG-dNΦ (n = 3). Scale bar, 15 μm.
  - (D) FACS-sorted CD11b<sup>+</sup>FCRLS<sup>+</sup> MG-dNΦ containing Alexa488<sup>+</sup> dNs and MG-nΦ from the same injection site 16 hr later.
  - (E) Heatmap of affected genes in MG-dNΦ (n = 4) versus MG-nΦ (n = 4) 16 hr after injection with dNs. One of two individual experiments.
  - (F) Top 20 affected genes shown in (E). Bars: mRNA NanoString (nCounts) (mean ± s.e.m) detected in 100 μg total RNA. \*p < 0.05 by two-tailed Student's t test.
  - (G) qPCR validation of selected genes. Gene expression level normalized against *Gapdh* via ΔCt (n = 3–4/group). Results: mean normalized expression ± SEM. \*p < 0.05, \*\*p < 0.01, \*\*\*p < 0.001 by one-way ANOVA followed by Tukey's multiple-comparison post-hoc test.
  - (H) Volcano plot of 552 TMT-mass spectrometry-identified proteins highlighting changes in MG-dNΦ versus MG-nΦ. p < 0.05 by two-tailed Student's t test.
  - (I) Circos plot: connectivity map derived from the pairwise comparison of transcriptome data from mouse AD models, ALS and *Mfp2*<sup>-/-</sup>; aging and irradiation are shown in orange. Each line represents a pairwise dataset overlap, determined by GSEA analysis and filtered by p < 0.001.
- See also Figures S3, S4, and S5 and Tables S3 and S4.



(legend on next page)

miR-155 were suppressed in *Trem2*<sup>-/-</sup> MG-dNΦ microglia (Figures 5B and Figure S7B). Targeting TREM2 signaling in the facial nerve axotomy (FNA) model also ameliorated neuronal loss in *Trem2*<sup>-/-</sup> mice (Figure 5C). To determine whether TREM2 induced the MGnD phenotype in disease, we genetically ablated *Trem2* in APP-PS1 and SOD1 mice. NanoString profiling of brain microglia from APP-PS1:*Trem2*<sup>-/-</sup> mice showed suppression of seven inflammatory molecules (*Trem2*, *Axl*, *Clec7a*, *Csf1*, *Itgax*, *Cd34*, and *Apoe*), which were among the most upregulated genes in the common disease-associated signature (Figure 5D). Among 108 restored genes in APP-PS1:*Trem2*<sup>-/-</sup> mice, 54 were commonly suppressed homeostatic microglial genes in disease; these included *P2ry12*, *Tmem119*, *Gpr34*, *Olfml3*, *Csf1r*, *Mertk*, *Rhob*, *Cx3Cr1*, *Tgfb1*, and *Tgfb1* and transcriptional-factor-encoding genes such as *Mef2a*, *Mafb*, and *Sall1* (Figure 5D). Moreover, we confirmed the protein-level restoration of P2ry12 and suppression of Clec7a in microglia associated with Aβ plaques in APP-PS1:*Trem2*<sup>-/-</sup> mice as compared to APP-PS1 mice (Figures 5E–5G). Consistent with previous findings (Jay et al., 2015), the Aβ-plaque load was decreased in APP-PS1:*Trem2*<sup>-/-</sup> mice (Figure 5H). In SOD1:*Trem2*<sup>-/-</sup> microglia, among 36 downregulated inflammatory genes, 11 genes were common to the disease-associated signature. Among 240 restored genes in SOD1:*Trem2*<sup>-/-</sup> mice, 66 were commonly suppressed homeostatic genes (Figure 5I). Transcription factors such as those encoding *Mef2a*, *Mafb*, and *Sall1* and molecules involved in TGFβ signaling such as *Tgfb* and *Tgfb1*, which were restored in *Trem2*<sup>-/-</sup> microglia in disease, were restored in *Apoe*<sup>-/-</sup> MG-dNΦ microglia. Clec7a<sup>+</sup>P2ry12<sup>+</sup> microglia were detected in spinal cords of SOD1:*Trem2*<sup>+/−</sup> but not SOD1:*Trem2*<sup>-/-</sup> mice at 115 days of age (Figure 5J). Clec7a<sup>+</sup>P2ry12<sup>+</sup> homeostatic microglia were preserved in SOD1:*Trem2*<sup>-/-</sup> mice (Figures 5J–5L). Expression of miR-155 was not induced in SOD1:*Trem2*<sup>-/-</sup> mice (Figure 5M). We had previously found early induction of Apoe in SOD1 males before clinical onset (Butovsky et al., 2015). To determine the TREM2 gender-dependent regulation of microglia in SOD1 mice, we performed unbiased RNAseq of the same samples shown in Figure 5I. We found 279 commonly affected genes (cluster 2) and 3,214 gender-specific genes (575 genes in females [cluster 1] and 2,639 genes in males [cluster 3]) (Figure 5N and Table S6). In commonly affected genes, SOD1:*Trem2*<sup>+/−</sup> males show induction of Apoe as compared to female littermates (Figures 5O and 5P), which

is in line with our previous report (Butovsky et al., 2015). Genetic deletion of *Trem2* in males as compared to SOD1:*Trem2*<sup>-/-</sup> female littermates resulted in marked suppression of *Apoe* and restoration of master regulators of homeostatic microglia; such regulators included those encoded by *Spi1* (PU.1), *Smad3*, *Tgfb1*, and *Sall1* (Figure 5P).

To validate TREM2 in regulating the microglial phenotypic switch in disease, we used GSEA to determine that transcripts from 5XFAD:*Trem2*<sup>-/-</sup> mice were enriched for the TREM2 responsive gene signature (Figures S7C–S7F and Table S6). Among the four disease models, TREM2-induced genes, including *Clec7a*, *Gpnmb*, *Fabp5*, *Lgals3*, *Csf1*, and *Ch25*, were also induced by *Apoe* (Table S5).

To investigate whether findings in APP-PS1:*Trem2*<sup>-/-</sup> mice were found in AD subjects carrying AD-associated TREM2 variants (AD-TREM2), we compared heterozygous carriers of R47H (AD-TREM2<sup>R47H</sup>) and R62H (AD-TREM2<sup>R62H</sup>) to common-variant AD-patients (AD-TREM2<sup>WT</sup>). In line with experimental data in mice (Wang et al., 2015), we found that microglia were more evenly distributed within the cortex in AD-TREM2 in both types of mutations and did not cluster around Aβ plaques as in AD-TREM2<sup>WT</sup> (Figures 6A–6C). Moreover, TMEM119 intensity was significantly higher in both TREM2 mutation carriers (Figures 6D and 6E). Taken together, these results demonstrate that activation of APOE signaling by dNs is TREM2 mediates and regulates the microglial phenotypic switch in APP-PS1 and SOD1 mice.

### Activation of the APOE Pathway Suppresses the Tolerogenic Function of Microglia

Genetic targeting of *Apoe* reduces neuroinflammation and disease in EAE (Shin et al., 2014). We tested the ability of microglia to inhibit T cell proliferation ex vivo because this has previously been reported as a tolerogenic function (Bai et al., 2009). CSFE-labeled T cells were stimulated in vitro with anti-CD3 and anti-CD28 mAbs (Figure 7A). M0 homeostatic microglia from the spinal cord of naive mice suppressed T cell proliferation. Stimulation of microglia with recombinant *Apoe* (rApoe) abrogated tolerogenic function of microglia. rApoe did not affect T cell proliferation in the absence of microglia (Figures 7A and 7B). Nonetheless, MGnD microglia from peak EAE was associated with the highest expression of *Apoe* (Figures 1B and 1C) and were unable to suppress T cell proliferation (Figures 7C and 7D). We then induced EAE in WT and *Apoe*<sup>-/-</sup> mice and

**Figure 4. APOE Regulates Transcriptional and Post-transcriptional Program of MGnD Phenotype**

(A) K-means clustering (K = 4) of 2,234 affected genes in bulk microglia (1,000 cells per animal) from WT and *Apoe*<sup>-/-</sup> mice. Vertical lane: mean of biological replicates of 1,000 MG-nΦ versus MG-dNΦ cells from WT (n = 10) versus *Apoe*<sup>-/-</sup> mice for MG-nΦ (n = 10) and MG-dNΦ (n = 9). Microglia isolated 16 hr after injection of dNs.

(B–E) Selected Apoe-induced genes (B), Apoe-induced Transcription Factors (TFs) (C), Apoe-repressed genes (D) and Apoe-repressed TFs (E) from WT and *Apoe*<sup>-/-</sup> mice 16 hr after injection of dNs. Means ± SEM are shown. \*p < 0.05, \*\*p < 0.01, \*\*\*p < 0.001 by one-way ANOVA followed by Tukey's multiple-comparison post-hoc test.

(F) qPCR validation of selected genes in MG-dNΦ from *Cx3cr1*<sup>CreERT2</sup>:*Apoe*<sup>f/f</sup> versus *Cx3cr1*<sup>w/w</sup>:*Apoe*<sup>f/f</sup> controls. Expression levels normalized against *Gapdh* via ΔCt (n = 6–10/group). Mean normalized expression ± SEM is shown. \*p < 0.05, \*\*p < 0.01, by two-tailed Student's t test.

(G) qPCR validation of genes in MG-nΦ from *Cx3cr1*<sup>CreERT2</sup>:*Apoe*<sup>f/f</sup> versus *Cx3cr1*<sup>w/w</sup>:*Apoe*<sup>f/f</sup> controls. Expression level normalized against *Gapdh* via ΔCt (n = 6–10/group). Mean normalized expression ± SEM is shown. \*p < 0.05, \*\*p < 0.01, by two-tailed Student's t test.

(H) Staining for NeuN<sup>+</sup> and P2ry12<sup>+</sup> in contralateral versus axotomized facial motor nucleus 7 days after surgery in WT (n = 5) versus *Apoe*<sup>-/-</sup> (n = 5) versus *Cx3cr1*<sup>CreERT2</sup>:*Apoe*<sup>f/f</sup> (n = 4) versus *Cx3cr1*<sup>w/w</sup>:*Apoe*<sup>f/f</sup> (n = 4) control mice. Scale bar, 80 μm.

(I) Quantification of NeuN<sup>+</sup> per facial motor nucleus in contralateral versus axotomized nucleus 7 days after surgery (n = 5). Means ± SEM are shown. \*p < 0.05, \*\*p < 0.01, \*\*\*p < 0.0001 by one-way ANOVA followed by Tukey's multiple-comparison post-hoc test.

See also Figure S6 and Table S5.

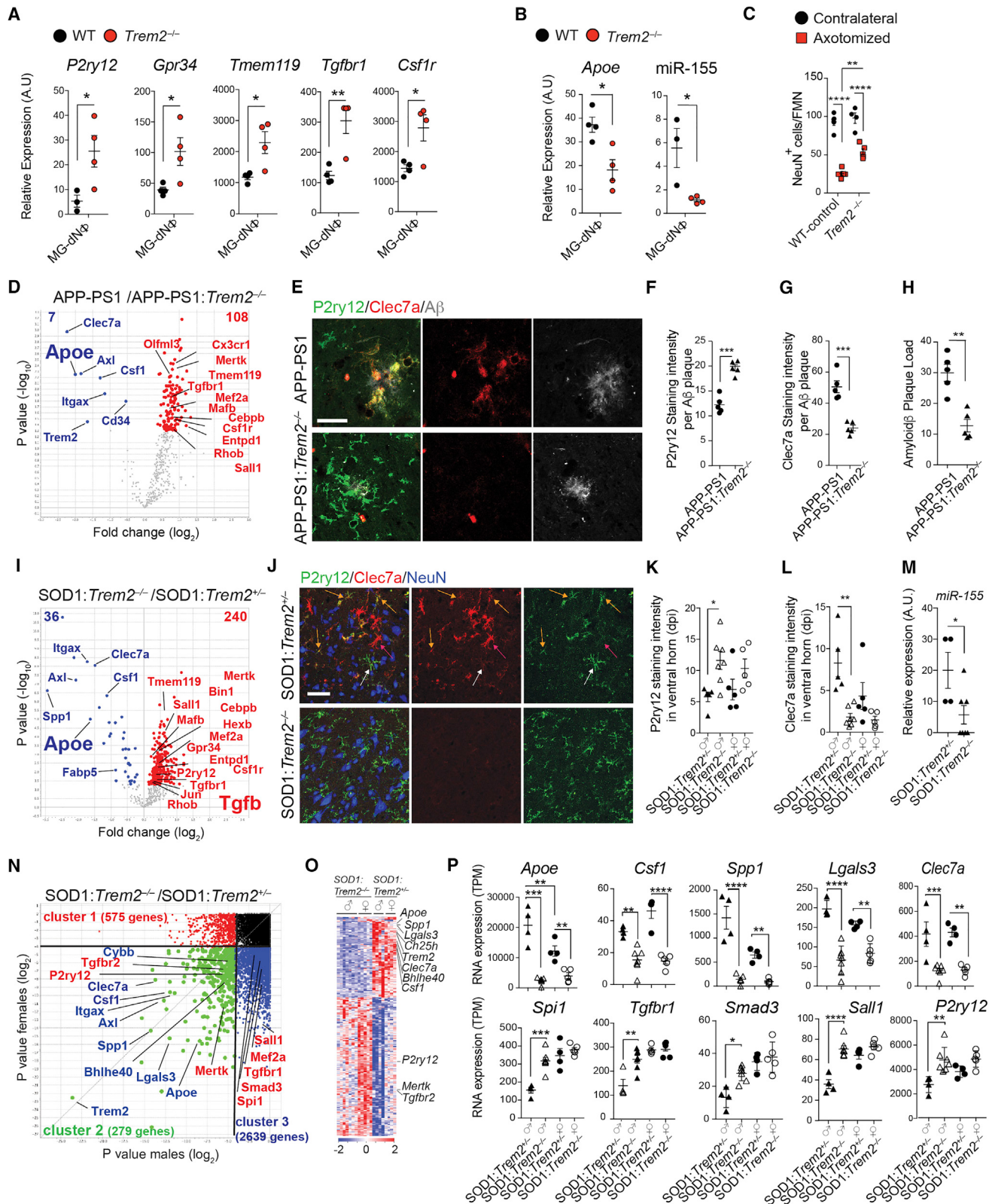


**Figure 5. Genetic Targeting of Trem2 Suppresses APOE Pathway and Restores the Homeostatic Microglia in APP-PS1 and SOD1 Mice**

(A) qPCR analysis of homeostatic genes in MG-dNΦ from Trem2<sup>-/-</sup> versus WT mice ( $n = 4$ ). Means  $\pm$  SEM are shown. \* $p < 0.05$ , \*\* $p < 0.01$  by one-way ANOVA.

(legend continued on next page)

found that, unlike WT-EAE microglia, *Apoe*<sup>-/-</sup> microglia from the spinal cord at disease peak suppressed T cell proliferation (Figures 7E and 7F), demonstrating the maintenance of the tolerogenic function. De novo stimulation of *Apoe*<sup>-/-</sup> microglia from EAE mice with rApoe inhibited their tolerogenic function (Figures 7G and 7H). Moreover, microglia isolated from SOD1 mice at disease peak, which show the highest expression of *Apoe* (Figure 1B), were also unable to suppress T cell proliferation (Figures 7I and 7J). In summary, we observed a loss of the tolerogenic function of microglia at peak EAE and in SOD1 mice. This loss was regulated by *Apoe*-dependent transcriptional effects in microglia.

## DISCUSSION

We identified a molecular signature of disease-associated microglia (MGnD) and found that this signature is dependent on the TREM2-APOE pathway. The MGnD phenotype was seen in several neurodegenerative models and was induced by phagocytosis of apoptotic neurons. In a mouse model and in human AD, neuritic A $\beta$ -plaque-associated microglia showed a MGnD phenotype consistent with reports of senescent microglia in aging and AD (Streit et al., 2009). These microglia lose some function including TGF $\beta$  signaling (Hickman et al., 2013). Apoptotic cells are efficiently phagocytosed during nervous system development (Jacobson et al., 1997). We reported that during early stages of development microglia induce *Apoe* expression, which is inversely correlated with the suppression of homeostatic genes (Butovsky et al., 2014). Thus, microglia during development and in neurodegenerative processes might share common modulatory mechanisms induced by apoptotic neurons. Neuronal apoptosis is a rare event in human AD (Stadelmann et al., 1999). However, focal apoptosis (synaptosis and necroptosis) associated with phosphatidylserine exposure

commonly occurs on neuronal processes, dendrites, or synapses (Mattson et al., 1998; Ofengeim et al., 2015). We found that dNs triggered the TREM2-APOE pathway to induce MG-dN $\Phi$  and suppress the homeostatic signature, which is tightly regulated by the TGF $\beta$  pathway (Butovsky et al., 2014; Gosselin et al., 2014).

We report a role for APOE in regulating the MGnD microglial subset in a cell-autonomous manner. Senile plaques contain dystrophic neurites (Grutzendler et al., 2007), and microglia engulf amyloid fibers (Dickson et al., 1988). We suggest that MGnD microglia, amyloid plaques, and dystrophic neurites form a microenvironment highly enriched in APOE, which could play a major role in AD progression. APOE both accumulates in amyloid plaques and facilitates A $\beta$  aggregation (Kim et al., 2012). Along with APOE induction, we found increased expression of APP in EAE microglia. Chiu et al. reported increased APOE and APP expression in SOD1 microglia (Chiu et al., 2013), and Huang et al. showed that APOE stimulates APP and increases amyloid- $\beta$  load in AD (Huang et al., 2017). Similarly, we found that A $\beta$ -plaque-associated microglia express a high level of APP in APP-PS1 mice. Our results are consistent with a report that increased APOE in CSF is associated with cognitive decline (Toledo et al., 2014). Thus, microglial APOE might play a detrimental role in AD.

Transcriptome profiling of disease-associated and homeostatic genes in microglia during aging and disease progression in SOD1, APP-PS1, and EAE identified APOE and TGF $\beta$  as the major upstream regulators of MGnD microglia. This phenotype was associated with neuritic plaques in APP-PS1 mice. Microglia acquire an MGnD phenotype after phagocytosis of dNs. Interestingly, the LPS- and IFN- $\gamma$ -induced (previously named M1) phenotype overlaps to some extent the MGnD microglia phenotype. However, microglia activated with LPS and IFN- $\gamma$  suppressed *Apoe* and induced *Egr1*, both of which are

- (B) qPCR analysis of *Apoe* and miR-155 expression in MG-dN $\Phi$  from *Trem2*<sup>-/-</sup> versus WT mice (n = 3–4/group). Means  $\pm$  SEM are shown. Data are normalized against *Gapdh* and U6 expression via  $\Delta\text{Ct}$ . \*p < 0.05 by two-tailed Student's t test.
- (C) Quantification of NeuN $^+$  per facial motor nucleus in contralateral versus axotomized nucleus in WT versus *Trem2*<sup>-/-</sup> (n = 4–5/group), 7 days after surgery. Means  $\pm$  SEM are shown. \*p < 0.05, \*\*p < 0.01, \*\*\*p < 0.0001 by one-way ANOVA followed by Tukey's multiple-comparison post-hoc test.
- (D) Volcano plot based on differentially expressed genes in microglia from APP-PS1 (n = 4) versus APP-PS1:*Trem2*<sup>-/-</sup> (n = 5) mice at 120 days. p < 0.05 by two-tailed Student's t test. Selected restored homeostatic (red) and suppressed inflammatory (blue) genes.
- (E) Staining for P2ry12, Clec7a, and A $\beta$  plaques in APP-PS1 versus APP-PS1:*Trem2*<sup>-/-</sup> mice (120 days). Scale bar, 20  $\mu\text{m}$ .
- (F and G) Quantification of P2ry12 and Clec7a intensity per A $\beta$  plaque in APP-PS1 versus APP-PS1:*Trem2*<sup>-/-</sup> mice (n = 5; 120 days). \*\*\*p < 0.001, by two-tailed Student's t test.
- (H) Quantification of A $\beta$ -plaque load per animal in APP-PS1 versus APP-PS1:*Trem2*<sup>-/-</sup> mice (n = 5; 120 days). \*\*p < 0.01, by two-tailed Student's t test.
- (I) Volcano plot based on differentially expressed genes in microglia from SOD1:*Trem2*<sup>-/-</sup> (n = 9) versus SOD1:*Trem2*<sup>-/-</sup> (n = 13) mice at 115 days (neurological score: 1). p < 0.05 by two-tailed Student's t test.
- (J) Staining for P2ry12, Clec7a, and NeuN in SOD1:*Trem2*<sup>+/-</sup> versus SOD1:*Trem2*<sup>-/-</sup> mice (lumbar section, 115 days). M0 homeostatic microglia (white arrows). MGnD microglia transitioning to MGnD (yellow arrows). MGnD at the epicenter of the ventral horn (red arrows). Scale bar, 50  $\mu\text{m}$ .
- (K and L) Quantification of P2ry12 and Clec7a intensity in ventral horn of SOD1:*Trem2*<sup>+/-</sup> (n = 4, n = 5 females) versus SOD1:*Trem2*<sup>-/-</sup> (n = 7 males, 5 females) mice (lumbar section, 115 days). \*\*p < 0.001, \*\*\*p < 0.001 by two-tailed Student's t test.
- (M) qPCR analysis of miR-155 expression in microglia isolated from the ventral horn of SOD1:*Trem2*<sup>+/-</sup> (n = 4) versus SOD1:*Trem2*<sup>-/-</sup> (n = 5) mice (lumbar section, 115 days). Means  $\pm$  SEM are shown. Data are normalized against U6 expression via  $\Delta\text{Ct}$ . \*p < 0.05 by two-tailed Student's t test.
- (N) Volcano plot: differentially expressed genes in spinal-cord microglia from male and female SOD1:*Trem2*<sup>+/-</sup> (n = 4 males, 4 females) versus SOD1:*Trem2*<sup>-/-</sup> (n = 7 males, 5 females) mice at 115 days (neurological score: 1). p < 0.05 by two-tailed Student's t test. Cluster 1: female-specific differentially expressed genes. Cluster 2: differentially expressed genes in both genders. Cluster 3: male-specific differentially expressed genes.
- (O) Heatmap of affected genes in male and female SOD1:*Trem2*<sup>+/-</sup> (n = 4 males, 4 females) versus SOD1:*Trem2*<sup>-/-</sup> (n = 7 males, 5 females) at 115 days (cluster 2). Vertical lanes: biological replicates per genotype and gender.
- (P) Gender comparison of homeostatic (lower panel) and MGnD genes (upper panel) from SOD1:*Trem2*<sup>+/-</sup> and SOD1:*Trem2*<sup>-/-</sup> mice (n = 4–7/group). Data represent means  $\pm$  SEM. \*p < 0.05, \*\*p < 0.01, \*\*\*p < 0.001, \*\*\*\*p < 0.0001 by one-way ANOVA followed by Tukey's multiple-comparison post-hoc test.
- See also Table S6.

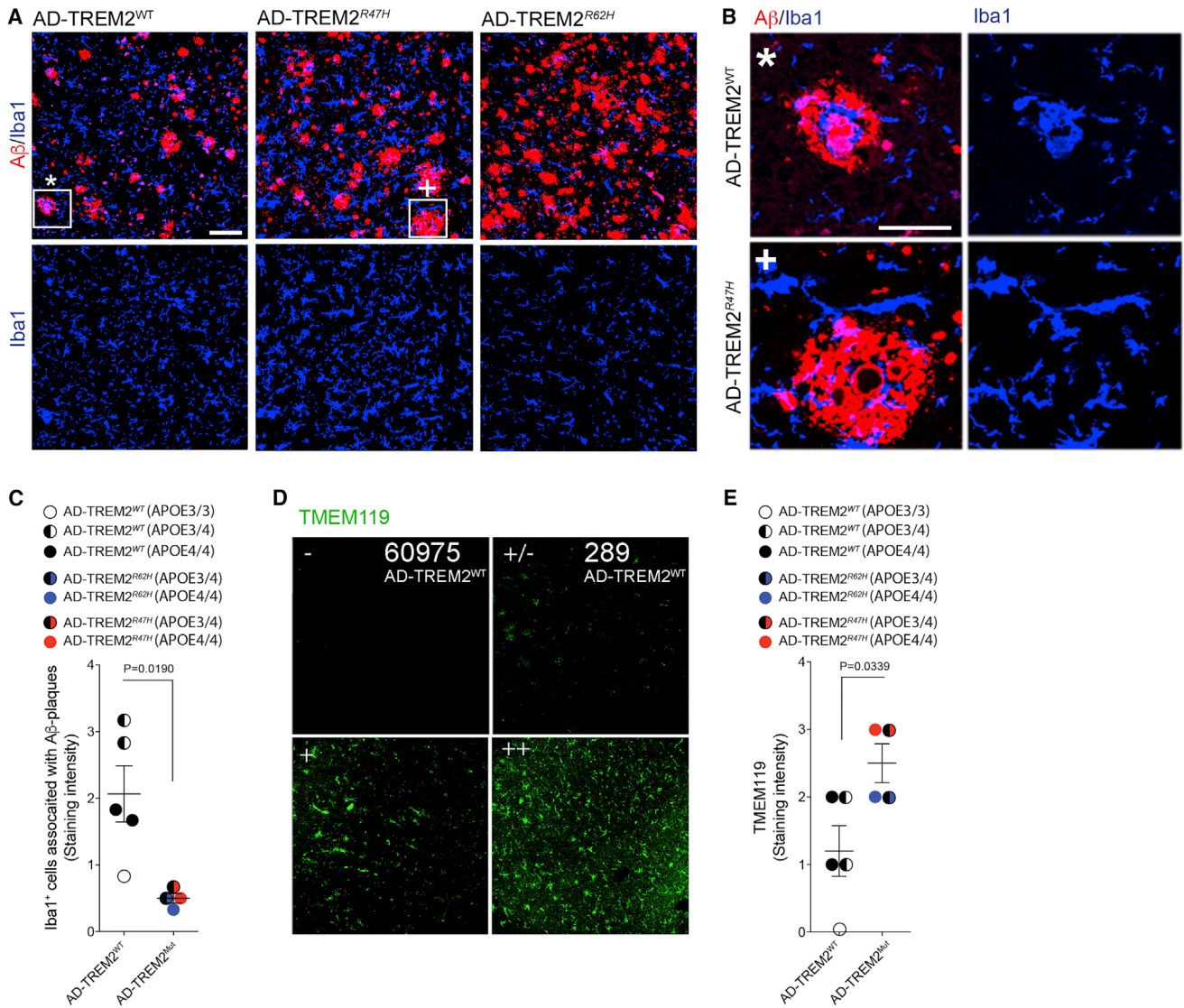


**Figure 6. TREM2 Haplodeficiency in Human AD Leads to Preservation of Microglia Morphology and TMEM119 Immunoreactivity**

(A) Staining for A $\beta$  (red) and IBA1 (blue) in AD control subjects (AD-TREM2<sup>WT</sup>, n = 6) and TREM2 variant carriers (AD-TREM2<sup>R47H</sup>, n = 2 and AD-TREM2<sup>R62H</sup>, n = 2). Lower panels: single distribution of IBA1<sup>+</sup> microglia in the same section areas. Scale bar, 100  $\mu$ m.

(B) Higher magnification of the plaques indicated by \* and + in (A). Scale bar, 50  $\mu$ m.

(C) Quantification of IBA1<sup>+</sup> microglia associated with A $\beta$  plaques in AD-TREM2<sup>WT</sup> and AD-TREM2<sup>Mut</sup> cortical tissue. Two-tailed Student's t test.

(D) Cortical tissue from AD-TREM2<sup>WT</sup> and AD-TREM2<sup>R62H</sup> cases stained with TMEM119. Panels show basis for scoring microglia staining, described in (E). Scores: – no cells stained; +/- single cells stained; + moderate number of microglia with TMEM119 reactivity; and ++ most microglia are TMEM119 positive.

(E) Quantification of TMEM119 in AD-TREM2<sup>WT</sup> and AD-TREM2<sup>Mut</sup> cortical tissue. TMEM119 expression in microglia rated as in (D); the ratings are shown in numbers: – (0), +/- (1), + (2), ++ (3). Two-tailed Student's t test.

See also Table S7.

reciprocally induced and suppressed in MGnD and MG-dNF microglia. Macrophage-lineage-determining factor PU.1 (Heinz et al., 2010) cooperates with microglia-specific enhancer regions of the Mef2 family (Butovsky et al., 2014; Matcovitch-Natan et al., 2016). Mef2a might partner with PU.1 to establish a microglia-specific signature (Lavin et al., 2014). Motif analysis of PU.1 binding revealed enrichment for Smad3, Mef2, and MafB consensus sequences, which cooperate with PU.1 to establish microglia-specific enhancer profiles, including TGF $\beta$  signaling (Butovsky

et al., 2014; Gosselin et al., 2014; Matcovitch-Natan et al., 2016). We found that APOE signaling suppresses PU.1, MEF2a, SMAD3, and TGF $\beta$  signaling. Deletion of Apoe in phagocytic microglia showed cell-autonomous regulation of the phenotypic switch. miR-155 is a major pro-inflammatory miRNA in ALS and the SOD1 model (Butovsky et al., 2012). Targeting miR-155 restored homeostatic microglia and attenuated disease in SOD1 mice (Butovsky et al., 2015). Here, we show that APOE signaling induces miR-155 in MGnD microglia. Targeting

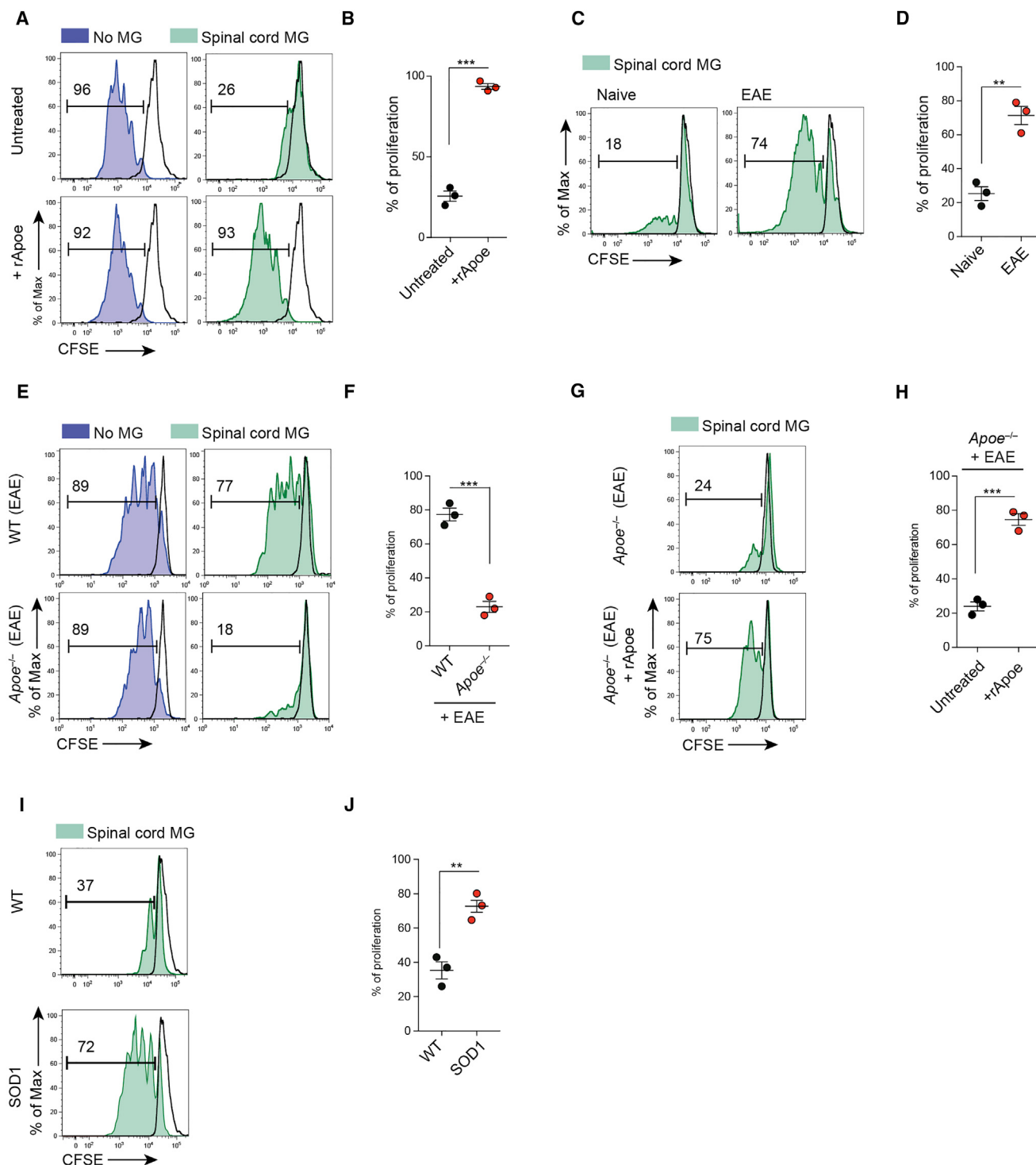


**Figure 7. Activation of APOE Pathway Suppresses Tolerogenic Function in Microglia**

- (A) CFSE<sup>+</sup> CD3<sup>+</sup> T cells cultured with spinal cord microglia of WT-naive mice. Cultures treated with soluble rApoe (100 ng/ml) for 72 hr.
- (B) T cell proliferation: means ± SEM are shown \*\*\*p < 0.001, two-tailed Student's t test (n = 3).
- (C) CFSE<sup>+</sup> CD3<sup>+</sup> T cells cultured for 72 hr with spinal-cord microglia from naive or EAE mice at disease peak.
- (D) T cell proliferation: means ± SEM are shown \*\*p < 0.01, two-tailed Student's t test (n = 3).
- (E) CFSE<sup>+</sup> CD3<sup>+</sup> T cells cultured for 72 hr with spinal-cord microglia from EAE WT versus Apoe<sup>-/-</sup> mice at disease peak.
- (F) T cell proliferation: means ± SEM are shown \*\*\*p < 0.001, two-tailed Student's t test (n = 3).

(legend continued on next page)

TREM2-APOE signaling in phagocytic microglia and in SOD1 mice suppressed miR-155 expression. Studies have shown that miR-155 directly targets Mef2a (Seok et al., 2011) and PU.1 (Lu et al., 2014). Together, these data suggest that TREM2-APOE signaling via miR-155 regulates microglia enhancers, and this regulation governs the core microglia-specific molecular signature.

Although TREM2 polymorphisms are associated with a risk of late-onset AD (Guerreiro et al., 2013), their role in neurodegenerative diseases is controversial. Wang et al. showed that deletion of TREM2 in 5XFAD mice, another model of AD, reduced A $\beta$  accumulation as a result of a dysfunctional response of microglia to cluster around A $\beta$  plaques (Wang et al., 2015). However, Jay et al. showed that TREM2 deficiency resulted in reduced infiltration of inflammatory myeloid cells and thereby ameliorated AD pathology (Jay et al., 2015) at early stages and exacerbated it at later stages (Jay et al., 2017). Subsequently, Wang et al. showed that amyloid-associated myeloid cells are derived from brain-resident microglia rather than from recruited peripheral monocytes (Wang et al., 2016). We found that genetic targeting of *Trem2* in APP-PS1 mice at early stages restored homeostatic microglia associated with the reduction of A $\beta$  plaques. In line with previous reports in mice and humans (Wang et al., 2015; Yuan et al., 2016), we found that microglia did not cluster around A $\beta$  plaques in TREM2-haplodeficient AD subjects. However, TMEM119 homeostatic microglia were more preserved in AD-TREM2 variants than in common-variant AD subjects, a result similar to the findings in APP-PS1:*Trem2*<sup>-/-</sup> mice. Consistent with our report, increased *TREM2* expression is associated with the *CD33* AD risk allele (Chan et al., 2015), and recent data showed that soluble TREM2 in the CSF is increased in the early symptomatic phase of AD in association with neuronal injury markers (Suárez -Calvet et al., 2016). This might reflect a dysregulation of homeostatic microglia in response to neuronal injury.

Keren-Shaul et al. reported that APOE induction is TREM2-independent in 5XFAD mice (Keren-Shaul et al., 2017), although a previous study (Wang et al., 2016) found that *Apoe* expression in 5XFAD mice was moderately lower than in WT mice. We found that genetic targeting of *Trem2* suppresses the APOE pathway and restores homeostatic microglia in APP-PS1 and SOD1 mice. As a ligand for TREM2 in microglia, APOE binds to dNs and increases *Trem2*-mediated phagocytosis (Atagi et al., 2015). We found that APOE ligand suppresses major transcription factors of homeostatic microglia. Future studies will determine whether the effect is TREM2 dependent. We identified TREM2 gender-dependent regulation of microglia in SOD1 mice; such regulation was not addressed by Wang et al. or Keren-Shaul et al.

We propose that the consequence of activating the TREM2-APOE pathway is the loss of the ability of MGnD microglia to pre-

vent neuronal loss and provide tolerogenic signals to T cells. In the context of MS, this would amplify the pro-inflammatory properties of T cells. MGnD microglia might also be protective and constitute an initial response to neuronal injury. As we showed recently, TREM2 deficiency might lock microglia in a homeostatic state (Mazaheri et al., 2017) and block essential defense functions of microglia during disease progression. In summary, we demonstrate that the TREM2-APOE pathway induces a microglia phenotypic switch from a homeostatic to neurodegenerative phenotype. The modulation of the microglial neurodegenerative phenotype through targeting of the TREM2-APOE pathway might serve as a way to restore homeostatic microglia and treat neurodegenerative disorders.

## STAR★METHODS

Detailed methods are provided in the online version of this paper and include the following:

- KEY RESOURCES TABLE
- CONTACT FOR REAGENT AND RESOURCE SHARING
- EXPERIMENTAL MODEL AND SUBJECT DETAILS
  - Mice
  - Human Specimens
- METHOD DETAILS
  - Scoring of SOD1 Mice
  - Conditional Genetic Deletion of *Apoe* in Microglia
  - Generation of Chimeric Mice
  - Immunohistochemistry
  - Analysis of P2RY12 and Dystrophic Axons in AD Brains
  - Induction of EAE
  - Isolation of Primary Neurons
  - Induction of Apoptosis and Labeling of Neurons
  - Induction of Necrosis in Neurons
  - Stereotactic Injections
  - Intrahippocampal Injection of Kainic Acid
  - Facial Nerve Axiotomy
  - Mouse Microglia Isolation and Sorting
  - Isolation of Spleenic CD11b<sup>+</sup>Ly6C<sup>+</sup> Monocytes
  - Mass Spectrometry Analysis
  - RNA Isolation and NanoString RNA Counting
  - Quantitative Real-Time PCR
  - Mouse MG550 Chip Design
  - NanoString Data Analysis
  - RNA Sequencing
  - In Vitro Suppression Assay
  - Heatmaps
  - Circos Plot
  - Ingenuity Pathway Analysis
- QUANTIFICATION AND STATISTICAL ANALYSIS
- DATA AND SOFTWARE AVAILABILITY

(G) CFSE<sup>+</sup>CD3<sup>+</sup> T cells cultured for 72 hr with spinal-cord microglia from EAE *Apoe*<sup>-/-</sup> mice at disease peak. Cultures treated with soluble rApoe (100 ng) for 72 hr.

(H) T cell proliferation: means  $\pm$  SEM are shown \*\*\*p < 0.001, two-tailed Student's t test (n = 3).

(I) CFSE<sup>+</sup>CD3<sup>+</sup> T cells cultured for 72 hr with spinal-cord microglia from WT versus SOD1 mice at disease peak (neurologic score: 4).

(J) T cell proliferation: means  $\pm$  SEM are shown \*\*p < 0.01, two-tailed Student's t test (n = 3). Black line: isotype control. Numbers on FACS plots: representative T cell proliferation (%).

Data are representative of three independent experiments (A–J).

**SUPPLEMENTAL INFORMATION**

Supplemental Information includes seven figures and seven tables and can be found with this article online at <http://dx.doi.org/10.1016/j.jimmuni.2017.08.008>.

**AUTHOR CONTRIBUTIONS**

O.B., S.K., C.M.: conceived study. S.K., C.M.: performed experiments, analyzed data, experimental design, writing. R.C.: NanoString analysis, LPS-injection. C.B.: isolated AD microglia for RNASEq, histology, imaging. N.C.: SOD1:*Trem2*<sup>-/-</sup> mice. L.B.: nerve axotomy, imaging, analysis. E.O., Z.F., D.J.G., G.T., K.H., Z.H., S.T.S.: performed experiments. REIF: neuronal culture. P.C.S., M.G., J.O.: T cell assays. D.H., J.U.: human AD-TREM2 variants. H.L., T.Z.: histology. C.L.: APP-PS1 experiments. A.W., J.H.: *Apoe*<sup>flaxed</sup> mice. F.H., F.M., C.H.: APP-PS1:*Trem2*<sup>-/-</sup> mice. T.I.: analysis. B.B.: mass spec. V.L., Y.X.: network analysis. Z.W., H.C.: circos plot. E.T., A.M., C.M.: RNaseq analyses, k-means clustering. H.L.W.: design, editing. O.B.: design, analysis, wrote manuscript with input from all authors.

**ACKNOWLEDGMENTS**

This work was supported by grants from the following organizations to the indicated authors. O.B.: NIH National Institute of Neurological Disorders and Stroke (R01NS088137), NIH National Institute on Aging (NIH-NIA) (R01AG051812 and R01AG054672), National Multiple Sclerosis Society (5092A1), Amyotrophic Lateral Sclerosis Association (2087), Nancy Davis Foundation Faculty Award, Cure Alzheimer's Fund (2017APOE:Butovsky). H.L.W.: Department of Defense (AL120029), Thome Foundation (2011D002865), NIH-NIA (R01AG043975 and R01AG040092). C.H.: European Research Council (321366-Amyloid), Deutsche Forschungsgemeinschaft (DFG) (EXC 1010 SyNergy), Cure Alzheimer's Fund, MetLife Foundation Award. J.H.: DFG (SFB841). D.M.H.: P50AG05681, P01-AG0399. C.L.: NIH-NIA (R01AG040092). T.I.: NIH-NIA (RF1AG054199-01). M.G.: DFG (GRK1459, SFB877). H.L.: Austrian Science Foundation Project (P27744-B27). C.M.: National Multiple Sclerosis Society (postdoctoral fellowship). We thank Prize4Life, a nonprofit organization dedicated to the discovery of treatments and a cure for ALS; Marco Colonna for *Trem2*<sup>-/-</sup> mice; Microscopy Core Facility/Universitätsklinikum Hamburg-Eppendorf; Deneen Kozoriz for FACS sorting. C.H. is a Roche advisor and collaborator.

Received: March 2, 2017

Revised: July 6, 2017

Accepted: August 17, 2017

Published: September 19, 2017

**REFERENCES**

- Atagi, Y., Liu, C.C., Painter, M.M., Chen, X.F., Verbeeck, C., Zheng, H., Li, X., Rademakers, R., Kang, S.S., Xu, H., et al. (2015). Apolipoprotein E Is a Ligand for Triggering Receptor Expressed on Myeloid Cells 2 (TREM2). *J. Biol. Chem.* **290**, 26043–26050.
- Bai, B., Song, W., Ji, Y., Liu, X., Tian, L., Wang, C., Chen, D., Zhang, X., and Zhang, M. (2009). Microglia and microglia-like cell differentiated from DC inhibit CD4 T cell proliferation. *PLoS ONE* **4**, e7869.
- Boillée, S., Yamanaka, K., Lobsiger, C.S., Copeland, N.G., Jenkins, N.A., Kassiotis, G., Kollias, G., and Cleveland, D.W. (2006). Onset and progression in inherited ALS determined by motor neurons and microglia. *Science* **312**, 1389–1392.
- Butovsky, O., Siddiqui, S., Gabriely, G., Lanser, A.J., Dake, B., Murugaiyan, G., Doykan, C.E., Wu, P.M., Gali, R.R., Iyer, L.K., et al. (2012). Modulating inflammatory monocytes with a unique microRNA gene signature ameliorates murine ALS. *J. Clin. Invest.* **122**, 3063–3087.
- Butovsky, O., Jedrychowski, M.P., Moore, C.S., Cialic, R., Lanser, A.J., Gabriely, G., Koeglsperger, T., Dake, B., Wu, P.M., Doykan, C.E., et al. (2014). Identification of a unique TGF-β-dependent molecular and functional signature in microglia. *Nat. Neurosci.* **17**, 131–143.
- Butovsky, O., Jedrychowski, M.P., Cialic, R., Krasemann, S., Murugaiyan, G., Fanek, Z., Greco, D.J., Wu, P.M., Doykan, C.E., Kiner, O., et al. (2015). Targeting miR-155 restores abnormal microglia and attenuates disease in SOD1 mice. *Ann. Neurol.* **77**, 75–99.
- Buttgereit, A., Lelios, I., Yu, X., Vrohlings, M., Krakoski, N.R., Gautier, E.L., Nishinakamura, R., Becher, B., and Greter, M. (2016). Sall1 is a transcriptional regulator defining microglia identity and function. *Nat. Immunol.* **17**, 1397–1406.
- Chan, G., White, C.C., Winn, P.A., Cimpean, M., Replogle, J.M., Glick, L.R., Cuerdon, N.E., Ryan, K.J., Johnson, K.A., Schneider, J.A., et al. (2015). CD33 modulates TREM2: convergence of Alzheimer loci. *Nat. Neurosci.* **18**, 1556–1558.
- Chiu, I.M., Morimoto, E.T., Goodarzi, H., Liao, J.T., O'Keeffe, S., Phatnani, H.P., Muratet, M., Carroll, M.C., Levy, S., Tavazoie, S., et al. (2013). A neurodegeneration-specific gene-expression signature of acutely isolated microglia from an amyotrophic lateral sclerosis mouse model. *Cell Rep.* **4**, 385–401.
- Dickson, D.W., Farlo, J., Davies, P., Crystal, H., Fuld, P., and Yen, S.H. (1988). Alzheimer's disease. A double-labeling immunohistochemical study of senile plaques. *Am. J. Pathol.* **132**, 86–101.
- Gautier, E.L., Shay, T., Miller, J., Greter, M., Jakubzick, C., Ivanov, S., Helft, J., Chow, A., Elpek, K.G., Gordonov, S., et al.; Immunological Genome Consortium (2012). Gene-expression profiles and transcriptional regulatory pathways that underlie the identity and diversity of mouse tissue macrophages. *Nat. Immunol.* **13**, 1118–1128.
- Gosselin, D., Link, V.M., Romanoski, C.E., Fonseca, G.J., Eichenfield, D.Z., Spann, N.J., Stender, J.D., Chun, H.B., Garner, H., Geissmann, F., and Glass, C.K. (2014). Environment drives selection and function of enhancers controlling tissue-specific macrophage identities. *Cell* **159**, 1327–1340.
- Grutzendler, J., Helmin, K., Tsai, J., and Gan, W.B. (2007). Various dendritic abnormalities are associated with fibrillar amyloid deposits in Alzheimer's disease. *Ann. NY Acad. Sci.* **1097**, 30–39.
- Guerreiro, R., Wojtas, A., Bras, J., Carrasquillo, M., Rogeava, E., Majounie, E., Cruchaga, C., Sassi, C., Kauwe, J.S., Younkin, S., et al.; Alzheimer Genetic Analysis Group (2013). TREM2 variants in Alzheimer's disease. *N. Engl. J. Med.* **368**, 117–127.
- Heinz, S., Benner, C., Spann, N., Bertolino, E., Lin, Y.C., Laslo, P., Cheng, J.X., Murre, C., Singh, H., and Glass, C.K. (2010). Simple combinations of lineage-determining transcription factors prime cis-regulatory elements required for macrophage and B cell identities. *Mol. Cell* **38**, 576–589.
- Hickman, S.E., Kingery, N.D., Ohsumi, T.K., Borowsky, M.L., Wang, L.C., Means, T.K., and El Khoury, J. (2013). The microglial sensome revealed by direct RNA sequencing. *Nat. Neurosci.* **16**, 1896–1905.
- Holtzman, I.R., Raj, D.D., Miller, J.A., Schaafsma, W., Yin, Z., Brouwer, N., Wes, P.D., Möller, T., Orre, M., Kamphuis, W., et al. (2015). Induction of a common microglia gene expression signature by aging and neurodegenerative conditions: a co-expression meta-analysis. *Acta Neuropathol. Commun.* **3**, 31.
- Huang, Y.A., Zhou, B., Wernig, M., and Sudhof, T.C. (2017). ApoE2, ApoE3, and ApoE4 Differentially Stimulate APP Transcription and Abeta Secretion. *Cell* **168**, 427–441, e421.
- Jacobson, M.D., Weil, M., and Raff, M.C. (1997). Programmed cell death in animal development. *Cell* **88**, 347–354.
- Jay, T.R., Miller, C.M., Cheng, P.J., Graham, L.C., Bemiller, S., Broihier, M.L., Xu, G., Margevicius, D., Karlo, J.C., Sousa, G.L., et al. (2015). TREM2 deficiency eliminates TREM2+ inflammatory macrophages and ameliorates pathology in Alzheimer's disease mouse models. *J. Exp. Med.* **212**, 287–295.
- Jay, T.R., Hirsch, A.M., Broihier, M.L., Miller, C.M., Neilson, L.E., Ransohoff, R.M., Lamb, B.T., and Landreth, G.E. (2017). Disease Progression-Dependent Effects of TREM2 Deficiency in a Mouse Model of Alzheimer's Disease. *J. Neurosci.* **37**, 637–647.
- Keren-Shaul, H., Spinrad, A., Weiner, A., Matcovitch-Natan, O., Dvir-Szternfeld, R., Ulland, T.K., David, E., Baruch, K., Lara-Astaiso, D., Toth, B., et al. (2017). A Unique Microglia Type Associated with Restricting Development of Alzheimer's Disease. *Cell* **169**, 1276–1290, e1217.

- Kim, J., Eltorai, A.E., Jiang, H., Liao, F., Verghese, P.B., Kim, J., Stewart, F.R., Basak, J.M., and Holtzman, D.M. (2012). Anti-apoE immunotherapy inhibits amyloid accumulation in a transgenic mouse model of A $\beta$  amyloidosis. *J. Exp. Med.* 209, 2149–2156.
- Koopman, G., Reutelingsperger, C.P., Kuijten, G.A., Keehnen, R.M., Pals, S.T., and van Oers, M.H. (1994). Annexin V for flow cytometric detection of phosphatidylserine expression on B cells undergoing apoptosis. *Blood* 84, 1415–1420.
- Kostic, V., Jackson-Lewis, V., de Bilbao, F., Dubois-Dauphin, M., and Przedborski, S. (1997). Bcl-2: prolonging life in a transgenic mouse model of familial amyotrophic lateral sclerosis. *Science* 277, 559–562.
- Kreutzberg, G.W. (1996). Microglia: a sensor for pathological events in the CNS. *Trends Neurosci.* 19, 312–318.
- Larner, A.J. (1995). The cortical neuritic dystrophy of Alzheimer's disease: nature, significance, and possible pathogenesis. *Dementia* 6, 218–224.
- Lavin, Y., Winter, D., Blecher-Gonen, R., David, E., Keren-Shaul, H., Merad, M., Jung, S., and Amit, I. (2014). Tissue-resident macrophage enhancer landscapes are shaped by the local microenvironment. *Cell* 159, 1312–1326.
- Lévesque, M., and Avoli, M. (2013). The kainic acid model of temporal lobe epilepsy. *Neurosci. Biobehav. Rev.* 37, 2887–2899.
- Lu, D., Nakagawa, R., Lazzaro, S., Staudacher, P., Abreu-Goodger, C., Henley, T., Boiani, S., Leyland, R., Galloway, A., Andrews, S., et al. (2014). The miR-155-PU.1 axis acts on Pax5 to enable efficient terminal B cell differentiation. *J. Exp. Med.* 211, 2183–2198.
- Martinez, F.O., and Gordon, S. (2014). The M1 and M2 paradigm of macrophage activation: time for reassessment. *F1000Prime Rep.* 6, 13.
- Masliah, E., Mallory, M., Alford, M., Tanaka, S., and Hansen, L.A. (1998). Caspase dependent DNA fragmentation might be associated with excitotoxicity in Alzheimer disease. *J. Neuropathol. Exp. Neurol.* 57, 1041–1052.
- Matcovitch-Natan, O., Winter, D.R., Giladi, A., Vargas Aguilar, S., Spinrad, A., Sarrazin, S., Ben-Yehuda, H., David, E., Zelada González, F., Perrin, P., et al. (2016). Microglia development follows a stepwise program to regulate brain homeostasis. *Science* 353, aad8670.
- Mattson, M.P. (2000). Apoptosis in neurodegenerative disorders. *Nat. Rev. Mol. Cell Biol.* 1, 120–129.
- Mattson, M.P., Keller, J.N., and Begley, J.G. (1998). Evidence for synaptic apoptosis. *Exp. Neurol.* 153, 35–48.
- Mazaheri, F., Snaidero, N., Kleinberger, G., Madore, C., Daria, A., Werner, G., Krasemann, S., Capell, A., Trümbach, D., Wurst, W., et al. (2017). TREM2 deficiency impairs chemotaxis and microglial responses to neuronal injury. *EMBO Rep.* 18, 1186–1198.
- Nimmerjahn, A., Kirchhoff, F., and Helmchen, F. (2005). Resting microglial cells are highly dynamic surveillants of brain parenchyma in vivo. *Science* 308, 1314–1318.
- Ofengheim, D., Ito, Y., Najafov, A., Zhang, Y., Shan, B., DeWitt, J.P., Ye, J., Zhang, X., Chang, A., Vakifahmetoglu-Norberg, H., et al. (2015). Activation of necroptosis in multiple sclerosis. *Cell Rep.* 10, 1836–1849.
- Orre, M., Kamphuis, W., Osborn, L.M., Melief, J., Kooijman, L., Huitinga, I., Klooster, J., Bossers, K., and Hol, E.M. (2014). Acute isolation and transcriptome characterization of cortical astrocytes and microglia from young and aged mice. *Neurobiol. Aging* 35, 1–14.
- Perry, V.H., and Holmes, C. (2014). Microglial priming in neurodegenerative disease. *Nat. Rev. Neurol.* 10, 217–224.
- Picelli, S., Björklund, A.K., Faridani, O.R., Sagasser, S., Winberg, G., and Sandberg, R. (2013). Smart-seq2 for sensitive full-length transcriptome profiling in single cells. *Nat. Methods* 10, 1096–1098.
- Radde, R., Bolmont, T., Kaeser, S.A., Coomaraswamy, J., Lindau, D., Stoltze, L., Calhoun, M.E., Jäggi, F., Wolburg, H., Gengler, S., et al. (2006). Abeta42-driven cerebral amyloidosis in transgenic mice reveals early and robust pathology. *EMBO Rep.* 7, 940–946.
- Satoh, J., Kino, Y., Asahina, N., Takitani, M., Miyoshi, J., Ishida, T., and Saito, Y. (2016). TMEM119 marks a subset of microglia in the human brain. *Neuropathology* 36, 39–49.
- Seok, H.Y., Tatsuguchi, M., Callis, T.E., He, A., Pu, W.T., and Wang, D.Z. (2011). miR-155 inhibits expression of the MEF2A protein to repress skeletal muscle differentiation. *J. Biol. Chem.* 286, 35339–35346.
- Shin, S., Walz, K.A., Archambault, A.S., Sim, J., Bollman, B.P., Koenigsknecht-Talboo, J., Cross, A.H., Holtzman, D.M., and Wu, G.F. (2014). Apolipoprotein E mediation of neuro-inflammation in a murine model of multiple sclerosis. *J. Neuroimmunol.* 271, 8–17.
- Stadelmann, C., Deckwerth, T.L., Srinivasan, A., Bancher, C., Brück, W., Jellinger, K., and Lassmann, H. (1999). Activation of caspase-3 in single neurons and autophagic granules of granulovacuolar degeneration in Alzheimer's disease. Evidence for apoptotic cell death. *Am. J. Pathol.* 155, 1459–1466.
- Sternberger, N.H., Sternberger, L.A., and Ulrich, J. (1985). Aberrant neurofilament phosphorylation in Alzheimer disease. *Proc. Natl. Acad. Sci. USA* 82, 4274–4276.
- Streit, W.J., Braak, H., Xue, Q.S., and Bechmann, I. (2009). Dystrophic (senescent) rather than activated microglial cells are associated with tau pathology and likely precede neurodegeneration in Alzheimer's disease. *Acta Neuropathol.* 118, 475–485.
- Suárez-Calvet, M., Araque Caballero, M.A., Kleinberger, G., Bateman, R.J., Fagan, A.M., Morris, J.C., Levin, J., Danek, A., Ewers, M., and Haass, C.; Dominantly Inherited Alzheimer Network (2016). Early changes in CSF sTREM2 in dominantly inherited Alzheimer's disease occur after amyloid deposition and neuronal injury. *Sci. Transl. Med.* 8, 369ra178.
- Tay, T.L., Mai, D., Dautzenberg, J., Fernández-Klett, F., Lin, G., Sagar, Datta, M., Drougard, A., Stempf, T., Ardura-Fabregat, A., et al. (2017). A new fate mapping system reveals context-dependent random or clonal expansion of microglia. *Nat. Neurosci.* 20, 793–803.
- Toledo, J.B., Da, X., Weiner, M.W., Wolk, D.A., Xie, S.X., Arnold, S.E., Davatzikos, C., Shaw, L.M., and Trojanowski, J.Q.; Alzheimer's Disease Neuroimaging Initiative (2014). CSF Apo-E levels associate with cognitive decline and MRI changes. *Acta Neuropathol.* 127, 621–632.
- Trapnell, C., Roberts, A., Goff, L., Pertea, G., Kim, D., Kelley, D.R., Pimentel, H., Salzberg, S.L., Rinn, J.L., and Pachter, L. (2012). Differential gene and transcript expression analysis of RNA-seq experiments with TopHat and Cufflinks. *Nat. Protoc.* 7, 562–578.
- Turnbull, I.R., Gilfillan, S., Cella, M., Aoshi, T., Miller, M., Piccio, L., Hernandez, M., and Colonna, M. (2006). Cutting edge: TREM-2 attenuates macrophage activation. *J. Immunol.* 177, 3520–3524.
- Verheijden, S., Bottelbergs, A., Krysko, O., Krysko, D.V., Beckers, L., De Munter, S., Van Veldhoven, P.P., Wyns, S., Kulik, W., Nave, K.A., et al. (2013). Peroxisomal multifunctional protein-2 deficiency causes neuroinflammation and degeneration of Purkinje cells independent of very long chain fatty acid accumulation. *Neurobiol. Dis.* 58, 258–269.
- Wagner, T., Bartelt, A., Schlein, C., and Heeren, J. (2015). Genetic Dissection of Tissue-Specific Apolipoprotein E Function for Hypercholesterolemia and Diet-Induced Obesity. *PLoS ONE* 10, e0145102.
- Wang, Y., Cella, M., Mallinson, K., Ulrich, J.D., Young, K.L., Robinette, M.L., Gilfillan, S., Krishnan, G.M., Sudhakar, S., Zinselmeyer, B.H., et al. (2015). TREM2 lipid sensing sustains the microglial response in an Alzheimer's disease model. *Cell* 160, 1061–1071.
- Wang, Y., Ulland, T.K., Ulrich, J.D., Song, W., Tzaferis, J.A., Hole, J.T., Yuan, P., Mahan, T.E., Shi, Y., Gilfillan, S., et al. (2016). TREM2-mediated early microglial response limits diffusion and toxicity of amyloid plaques. *J. Exp. Med.* 213, 667–675.
- Xu, Q., Bernardo, A., Walker, D., Kanegawa, T., Mahley, R.W., and Huang, Y. (2006). Profile and regulation of apolipoprotein E (ApoE) expression in the CNS in mice with targeting of green fluorescent protein gene to the ApoE locus. *J. Neurosci.* 26, 4985–4994.
- Yuan, P., Condello, C., Keene, C.D., Wang, Y., Bird, T.D., Paul, S.M., Luo, W., Colonna, M., Baddeley, D., and Grutzendler, J. (2016). TREM2 Haplodeficiency in Mice and Humans Impairs the Microglia Barrier Function Leading to Decreased Amyloid Compaction and Severe Axonal Dystrophy. *Neuron* 92, 252–264.

## STAR★METHODS

## KEY RESOURCES TABLE

REAGENT or RESOURCE	SOURCE	IDENTIFIER
<b>Antibodies</b>		
Mouse monoclonal anti-NeuN (clone A60)	Millipore	Cat#MAB377
Rabbit polyclonal anti-Iba1	WAKO Chemicals	Cat#019-19741
Rabbit polyclonal anti-P2RY12	Butovsky et al., 2014	N/A
Rat-monoclonal microglia-specific 4D4	Butovsky et al., 2012	N/A
Rat monoclonal anti-P2RY12	This paper	N/A
Goat polyclonal anti-APOE	Millipore	Cat# AB947
Mouse monoclonal anti-phosphorylated neurofilament (clone SMI31)	BioLegend	Cat#801601
Rabbit polyclonal anti-human TMEM119	Sigma	Cat# HPA051870
Rabbit monoclonal [28-3] anti-mouse TMEM119	Abcam	Cat#ab209064
Rat monoclonal anti-Clec7a (clone R1-8g7)	Invivogene	Cat#mabg-mdect
Ly6C-FITC	BD Biosciences	Cat#553104
Rat-monoclonal anti-FCRLS (clone 4G11)	Butovsky et al., 2014	N/A
Mouse monoclonal anti-Amyloid $\beta$ (clone 6E10)	Covance	Cat#SIG-39320
Mouse monoclonal anti-Amyloid $\beta$ (clone BAM-10)	Zytomed	Cat#Mob 410-05
Mouse monoclonal anti-Amyloid $\beta$ (Clone W02)	Millipore	Cat#MABN10
Rat monoclonal anti-CD11b-PeCy7 (clone M1/70)	BD Biosciences	Cat#552850
Armenian Hamster monoclonal anti-CD3 (clone 145-2C11)	BioLegend	Cat#100302
Super Clonal anti-goat Alexa Fluor555	Thermo Fisher Scientific	Cat#A27017
<b>Biological Samples</b>		
Human cortical specimens	Massachusetts General Hospital	Massachusetts Alzheimer Disease Research Center (MADRC; NIA P50 AG005134)
Human Brain Autopsies (AD and Controls)	Center for Brain Research, Medical University of Vienna	Archival Collection; EK #: 535/2004/2017
Human Brain specimens (AD controls and AD Trem2-polymorphisms)	Washington University	Knight Alzheimer's Disease Research Center (NIA P50 AG0568)
<b>Chemicals, Peptides, and Recombinant Proteins</b>		
Annexin V	Biolegend	Cat#640901
7-AAD	Biolegend	Cat#420403
Tamoxifen	Sigma-Aldrich	Cat#T5648
TritonX-100	Roche	Cat#11332481001
Pierce Protein-Free T20 blocking buffer	Thermo Fisher Scientific	Cat#37571
DAPI-Fluoromount-G	Southern Biotech	Cat#0100-20
Fluoromount-G	Southern Biotech	Cat#0100-01
Antibody diluent	DAKO	Cat#S2022
Avidin peroxidase	Jackson	Cat#016-030-084
Tyramine	Sigma	Cat#T-7255
Gallate Geltol:	Invitrogen	Cat#15514-011
Glycerol	Calbiochem	Cat#475904
Moviol	Sigma	Cat#P-3130
Gallate		
Pertussis toxin	List Biological Laboratories	Cat#180
CFA Complete Freund Adjuvant	Difco	Cat#231131
myelin oligodendrocyte glycoprotein (MOG)35–55 peptide	Genemed Synthesis	Cat# MOG3555-P-5

(Continued on next page)

***Continued***

REAGENT or RESOURCE	SOURCE	IDENTIFIER
5(6)-Carboxyfluorescein N-hydroxysuccinimidyl ester	Thermo Fisher Scientific	Cat#C34554
LPS Lipopolysaccharide from Escherichia coli 0127:B8	Thermo Fisher Scientific	Cat#L3129
Mouse recombinant APOE (host: yeast)	My Biosource	Cat#MBS955382
pHrodo® Green Zymosan Bioparticles®	Life Technologies	Cat#P35365
Conjugate for Phagocytosis		
pHrodo® Green E. coli BioParticles®	Life Technologies	Cat#P35366
Conjugate for Phagocytosis		
Kainic Acid	Sigma-Aldrich	K0250-10MG
Fluoro-Jade C	Histo-chem	#1FJC
Alexa Fluor488 5-SDP Ester	Thermo Fisher Scientific (Molecular Probes)	Cat#A30052
Alexa Flour405 5-NHS Ester	Thermo Fisher Scientific (Molecular Probes)	Cat#A30000
Anhydrous DMSO	Thermo Fisher Scientific	Cat#D12345
<b>Critical Commercial Assays</b>		
mirVanaTM miRNA isolation kit	Ambion	Cat#AM1561
high-capacity cDNA Reverse Transcription Kit	Applied Biosystems	Cat#4368814
anti-CD11b magnetic beads	Miltenyi Biotec	Cat#130-049-601
T cell-activator CD3/CD28 magnetic beads	Thermo Fisher Scientific	Cat#11456D
Fc Receptor blocking anti-CD16/32 antibodies	BD Biosciences	Cat#553141
<b>Deposited Data</b>		
Gene expression data	GSE101689	N/A
Protein data	PeptideAtlas: PASS01081	N/A
<b>Experimental Models: Organisms/Strains</b>		
Mouse: C57Bl/6J	The Jackson Laboratory	JAX: 00664
Mouse: <i>Apoe</i> <sup>-/-</sup>	The Jackson Laboratory	JAX: 002052
Mouse: <i>miR-155</i> <sup>-/-</sup>	The Jackson Laboratory	JAX: 007745
Mouse: <i>Apoe</i> <sup>f/f</sup>	Wagner et al., 2015	N/A
Mouse: APP-PS1	Radde et al., 2006	N/A
Mouse: <i>Trem2</i> <sup>-/-</sup>	Turnbull et al., 2006	N/A
Mouse: Cx3cr1 <sup>CreERT2</sup>	The Jackson Laboratory	JAX: 021160
Mouse: SOD1 <sup>G93A</sup>	The Jackson Laboratory	JAX: 004435
<b>Oligonucleotides</b>		
<i>Apoe</i> (Mm01307193_g1)	Thermo Fisher Scientific	Cat#4331182
<i>Clec7a</i> (Mm01307193_g1)	Thermo Fisher Scientific	Cat#4331182
<i>Csf1r</i> (Mm01266652_m1)	Thermo Fisher Scientific	Cat#4331182
<i>Egr1</i> (Mm00656724_m1)	Thermo Fisher Scientific	Cat#4331182
<i>Gapdh</i> (Mm99999915_g1)	Thermo Fisher Scientific	Cat#4331182
<i>Gpr34</i> (Mm02620221_s1)	Thermo Fisher Scientific	Cat#4331182
<i>P2ry12</i> (Mm01950543_s1)	Thermo Fisher Scientific	Cat#4331182
<i>Tgfb1</i> (Mm01178820_m1)	Thermo Fisher Scientific	Cat#4331182
<i>Tgfbr1</i> (Mm00436964_m1)	Thermo Fisher Scientific	Cat#4331182
<i>Tmem119</i> (Mm00525305_m1)	Thermo Fisher Scientific	Cat#4331182
<i>miR-155</i> (RT002571)	Thermo Fisher Scientific	Cat#4427975
<i>U6</i> (RT001973)	Thermo Fisher Scientific	Cat#4427975
<b>Software and Algorithms</b>		
Leica application suite software (LAS-AF-lite)	Leica	<a href="http://www.leica-microsystems.com">http://www.leica-microsystems.com</a>
Ingenuity software	Ingenuity Systems	<a href="http://www.ingenuity.com">http://www.ingenuity.com</a>
Multiplot studio 1.5.20	GParc	<a href="http://gparc.org/">http://gparc.org/</a>

(Continued on next page)

**Continued**

REAGENT or RESOURCE	SOURCE	IDENTIFIER
GraphPad Prism 7	GraphPad Software	<a href="http://www.graphpad.com">http://www.graphpad.com</a>
FlowJo (version 10.0.8R1)	FlowJo	<a href="http://www.flowjo.com">http://www.flowjo.com</a>
Proteome Discoverer 2.1.0.81 software	Thermo Fisher Scientific	<a href="https://portal.thermo-brims.com/">https://portal.thermo-brims.com/</a>
Sequest HT algorithm	Thermo Fisher Scientific	<a href="https://portal.thermo-brims.com/">https://portal.thermo-brims.com/</a>
GSEA algorithm	N/A	<a href="http://software.broadinstitute.org/gsea/index.jsp">http://software.broadinstitute.org/gsea/index.jsp</a>
oPOSSUM	oPOSSUM	<a href="http://opossum.cisreg.ca/oPOSSUM3/">http://opossum.cisreg.ca/oPOSSUM3/</a>
Circos package 0.68.12	N/A	<a href="http://circos.ca/software/download/circos/">http://circos.ca/software/download/circos/</a>
R software (version 3.4.0)	N/A	<a href="https://cran.r-project.org/">https://cran.r-project.org/</a>
MeV software (version 10.2)	N/A	<a href="http://mev.tm4.org">http://mev.tm4.org</a>
Other		
NanoString nCounter MG400 chip	Butovsky et al., 2014	<a href="http://www.nanostring.com/">http://www.nanostring.com/</a>
NanoString nCounter MG468 chip	Butovsky et al., 2015	<a href="http://www.nanostring.com/">http://www.nanostring.com/</a>
NanoString nCounter MG550 chip	This paper	<a href="http://www.nanostring.com/">http://www.nanostring.com/</a>
LTQ Orbitrap Velos	Thermo Fisher Scientific	<a href="http://planetorbitrap.com/">http://planetorbitrap.com/</a>
C18 Reprosil resin (5 μm, 100 Å)	Dr. Maisch GmbH	<a href="http://www.dr-maisch.com/xedin.php">http://www.dr-maisch.com/xedin.php</a>
C18 Reprosil resin (1.8 μm, 200 Å)	Dr. Maisch GmbH	<a href="http://www.dr-maisch.com/xedin.php">http://www.dr-maisch.com/xedin.php</a>

**CONTACT FOR REAGENT AND RESOURCE SHARING**

Further information and requests for resources and reagents should be directed to and will be fulfilled by the Lead Contact, Oleg Butovsky ([obutovsky@rics.bwh.harvard.edu](mailto:obutovsky@rics.bwh.harvard.edu)).

**EXPERIMENTAL MODEL AND SUBJECT DETAILS****Mice**

C57BL/6J, B6.Cg-Tg(SOD1\*G93A)1Gur/J (SOD1<sup>G39A</sup>), B6.129P2-Apoe<sup>tm1Unc</sup>/J (Apoe<sup>-/-</sup>), B6.Cg-Mir155tm1.1Rsky/J (miR-155<sup>-/-</sup>), and B6.129P2(Cg)-Cx3cr1tm2.1(cre/ERT)Litt/WganJ (Cx3cr1<sup>CreERT2</sup>) mice were purchased from Jaxmice. Trem2<sup>-/-</sup> mice (Turnbull et al., 2006) were generously provided by Dr. Marco Colonna (Washington Univ.). APP-PS1 mice were kindly provided by Dr. Mathias Jucker (University of Tübingen). These mice develop amyloid plaque deposition approximately at six weeks of age in the neocortex. Deposits appear in the hippocampus at about three to four months, and in the striatum, thalamus, and brainstem at four to five months (Radde et al., 2006). These mice were analyzed at 9 and 24 months, respectively. APP-PS1:Trem2<sup>-/-</sup>, were generated by crossing APP-PS1 mice with Trem2<sup>-/-</sup> mice. These mice were analyzed at 4 months of age. Generation of Apoe<sup>f/f</sup> mice has been described recently (Wagner et al., 2015) and these mice were used for microglia specific deletion of Apoe. If not otherwise stated, mice were female and 6–8 weeks of age at the beginning of the experiments. Mice were housed under specific pathogen free conditions. Mice from different genotypes were cohoused. Mice did not undergo any procedures prior to their stated use. All mice were housed with food and water ad libitum. Mice were euthanized by CO<sub>2</sub> inhalation. The Institutional Animal Care and Use Committee at Harvard Medical School approved all experimental procedures involving animals.

**Human Specimens**

Cortex samples from AD patients and respective controls from Center for Brain Research, Medical University of Vienna were examined and chosen with identical settings and were investigated to determine the degree of P2ry12 abundance associated with either diffuse or neuritic plaques. Brain tissues from AD patients with and without mutations in TREM2 were sampled and characterized at the University of Washington by David Holtzman and his team (St. Louis). Beside age, gender and disease severity (Braak stage, estimated CDR), the APOE genotype was determined for each patient. The cases examined in this study are summarized in Table S7. Tissues were embedded in paraffin and paraffin sections were cut at a thickness of 8 μm. After deparaffination, tissue sections were stained as described in the immunohistochemistry section. All stains and subsequent analyses were performed blinded to the investigator. Use of post-mortem human brain tissue was approved by the Knight Alzheimer's Disease Research Center Biospecimens Committee. The approved use of post-mortem human brain tissue obtained through the Knight ADRC was exempt from the university human studies committee review (exemption numbers 89-055, 89-056). Written informed consent was obtained from participants in studies at the Knight Alzheimer's Disease Research center (P50 AG05681) and their collateral sources.

## METHOD DETAILS

### Scoring of SOD1 Mice

SOD1<sup>G39A</sup> mice were assessed clinically by monitoring body weight (3 times/week) and neurological score (daily) starting at day 60. Disease progression was documented according to established methodology provided by Prize4Life and The Jackson Laboratory. Symptomatic analysis was conducted by monitoring neurological score and weight starting at day 60, and symptomatic onset was defined as the age at which animals began to decline in weight (Boillée et al., 2006). The neurological score used a scale of 0 to 4 developed by ALSTDI. Criteria used to assign each score level were: 0 = Full extension of hind legs away from the lateral midline when the mouse is suspended by its tail, and mouse can hold this position for 2 s, suspended 2–3 times; 1 = Collapse or partial collapse of leg extension toward lateral midline (weakness) or trembling of hind legs during tail suspension; 2 = Curling of the toes and dragging of at least one limb during walking; 3 = Rigid paralysis or minimal joint movement, foot not being used for forward motion; 4 = Mouse cannot right itself within 30 s from either side. A score of 4 also corresponded with the humane endpoint of the study.

### Conditional Genetic Deletion of Apoe in Microglia

To induce Cre-recombinase expression, a dose of tamoxifen (75 mg/kg of body weight) in corn oil (Sigma) was injected i.p. for 5 consecutive days. For genetic depletion of APOE in microglia cells, *Apoe*<sup>f/f</sup> were crossed with tamoxifen-inducible *Cx3cr1*<sup>CreERT2</sup> transgenic mice. Recombination was induced in *Cx3cr1*<sup>CreERT2</sup>; *Apoe*<sup>f/f</sup> adult mice and *Cx3cr1*<sup>wt</sup>; *Apoe*<sup>f/f</sup> littermates were used as controls.

### Generation of Chimeric Mice

*Cx3cr1*:GFP<sup>+/−</sup> chimera mice were generated as previously described (Butovsky et al., 2014). In brief, 30-day-old C57BL/6J recipient mice protected by lead head shielding were lethally irradiated (950 Rad) and transplanted with bone marrow (BM) from *Cx3cr1*:GFP<sup>+/−</sup> donor mice. 8 weeks post-BM transplantation, EAE was induced in these chimera mice as described below.

### Immunohistochemistry

Following immersion fixation in 4% PFA, brains were dehydrated and embedded in paraffin. H&E staining was performed according to standard procedures. For immunohistochemical staining, frontal sections (2–5 µm) were collected on superfrost slides, deparaffinized in xylol and rehydrated. After heat induced antigen retrieval, the following primary antibodies were used for detection: Neurons, anti-NeuN (clone A60, Millipore, 2 µg ml<sup>−1</sup>), microglia/macrophages/monocytes, anti-Iba1 (polyclonal, #019-19741; WAKO Chemicals, 1 µg ml<sup>−1</sup>), resident microglia, anti-P2ry12 [polyclonal, 0.4 µg ml<sup>−1</sup>, validated in ref. (Butovsky et al., 2015; Butovsky et al., 2014)], anti-P2ry12 (monoclonal, 0.4 µg ml<sup>−1</sup>, validated in this study), microglia specific 4D4 (monoclonal, validated in ref. (Butovsky et al., 2012)), anti-Apoe (polyclonal, AB947; Millipore, 5 µg ml<sup>−1</sup>) phosphorylated neurofilament (pNF; (clone SMI31 Biolegend; 1:2,000), and anti-human TMEM119 antibody (Sigma, HPA051870; 1:300). Detection was performed with the respective secondary antibodies and diaminobenzidine.

For immunofluorescence staining, antigen retrieval was performed for 30 min at 96°C in 10 mM citrate buffer pH 6.0. Subsequently, sections were permeabilized with 0.2% Triton X-100 (Roche) in TBS for 5 min. Tissues were blocked in Pierce Protein-Free T20 blocking buffer (Thermo Scientific) and treated with 1% Sudan Black to reduce autofluorescence. Sections were incubated with the first antibody at 4°C overnight, washed with TBS Tween (TBS-T) and incubated with secondary donkey anti-rabbit Alexa555 antibody (Life Technologies, 6 µg ml<sup>−1</sup>) or chicken anti-rabbit Alexa488, anti-mouse Alexa647 (Life Technologies, 6 µg ml<sup>−1</sup>) during 90 min. Apoe was stained with goat anti-Apoe (polyclonal, Millipore, 5 µg ml<sup>−1</sup>) and detected with the superclonal rabbit anti-goat Alexa555 (Thermo Scientific, 1 µg ml<sup>−1</sup>). Sections were washed again and slides were mounted with DAPI-Fluoromount-G (SouthernBiotech, Birmingham, USA). Staining and analyses of tissues from APP-PS1:*Trem2*<sup>−/−</sup>, APP-PS1, WT, *Cx3cr1*<sup>wt</sup>; *Apoe*<sup>f/f</sup>, *Apoe*<sup>−/−</sup>, *Trem2*<sup>−/−</sup>, and *Cx3cr1*<sup>CreERT2</sup>; *Apoe*<sup>f/f</sup> mice were performed on cryo or floating sections and the following additional antibodies were used: anti-mouse Clec7a (clone R1-8g7, Invivogene, 1:30); anti-mouse TMEM119 (clone 28-3, Abcam, 1:100); anti-Aβ (clone 6E10, Covance, 1:100 or Mob 410-05, Zytomed, 1:100); goat anti-mouse Alexa405; chicken anti-rat Alexa488 or Alexa647. Anti-Aβ antibody (clone 6E10, Covance) was applied on cryo sections (30 µm) for staining in Figure 2a, only. Sections were permeabilized with 0.2% Triton X-100 as mentioned above with subsequent antibody incubations. Data acquisition and quantification was performed using a Leica TCS SP5 confocal microscope and Leica application suite software (LAS-AF-lite). Quantification of positive staining within microglia or amyloid β (Aβ)-plaque region was performed using the LAS-AF quantification tool. Briefly, the region of interest was carefully selected and the sum of the values of the pixels in the selection was calculated. For quantification of Apoe-signal in human microglia (paraffin sections 5 µm), only cells with fully visible cell bodies, away from plaques (stained with anti-Aβ antibody Mob 410-05, Zytomed) or astrocytes were used. Selected area was 300 µm<sup>2</sup> and 30 cells were measured each (n = 3 AD subjects versus n = 3 controls). To investigate selected protein expression profiles in APP-PS1 versus APP-PS1:*Trem2*<sup>−/−</sup> mouse brains, we used floating sections (30 µm). For quantification of Clec7a signal within single plaque (stained with anti-Aβ antibody Mob 410-05, Zytomed) associated microglia in mouse brains, we measured an area of 250 µm<sup>2</sup> from 10–14 plaques each in APP-PS1 (n = 5) and APP-PS1:*Trem2*<sup>−/−</sup> (n = 5) mice. P2ry12 protein expression in microglia associated with Aβ plaque area was measured in 3,000 µm<sup>2</sup> from 15 plaques per each animal in APP-PS1 (n = 5) and APP-PS1:*Trem2*<sup>−/−</sup> (n = 5) mice. For quantification of plaque burden, we stained for Aβ (anti-Aβ antibody Mob 410-05, Zytomed) and quantified the Aβ positive signal in the cortex of each mouse within an area of 600,000 µm<sup>2</sup>. For quantification of Clec7a and P2ry12 signal intensity in the ventral horn of SOD1: *Trem2*<sup>−/−</sup> (n = 13)

and SOD1:*Trem2*<sup>+/-</sup> ( $n = 9$ ) mice, 5 areas of  $3,600 \mu\text{m}^2$  were measured in 3 sections per spinal cord (cryo-sections  $30 \mu\text{m}$ ). For quantitative evaluation of P2RY12 and dystrophic axons in human AD brains (paraffin sections  $5 \mu\text{m}$ ), double staining for P2RY12 with A $\beta$  or phosphorylated neurofilament was performed on paraffin sections as described previously. After deparaffinization heat induced epitope retrieval was performed in EDTA buffer (pH: 8.5). The primary antibodies (rabbit polyclonal anti- P2RY12; mouse monoclonal anti-A $\beta$ , Clone W02, Millipore and mouse monoclonal anti-phosphorylated neurofilament, SMI31; Sternberger Monoclonals, Affiniti Res Prod.) were applied together overnight. Antibody binding was visualized with either alkaline phosphatase-conjugated anti-mouse antibodies or with biotinylated anti-rabbit secondary antibodies and peroxidase-conjugated streptavidin. Alkaline phosphatase or peroxidase reaction products were visualized by development with fast blue BB salt (blue) or amino ethyl carbazole (AEC; red), respectively.

Serial tissue sections from AD patients with and without mutations in TREM2 were stained by immunofluorescence double labeling with antibodies against IBA1, TMEM119, APOE (see above), and A $\beta$  (Clone W02, Millipore) in the following combinations: IBA1/A $\beta$  and TMEM119/APOE as described above. All quantifications were performed blinded to the researchers. For quantification of positive staining signal, six images through the cortical layers I-IV were taken with a 20x objective. Microglia clusters in A $\beta$  plaques were determined in sections double stained for A $\beta$  and Iba-1 and manually counted within 6 standardized images/case of ( $0.6 \text{ mm}^2$ ). Images were saved as tiff-format, converted into 8-bit greyscale in ImageJ and inverted. In the resulting images, the area fraction with positive signal was calculated and plotted as percentage of cortical area covered by amyloid deposits, APOE deposits or IBA1-signal in the respective graph. The association of Iba1 positive cells associated with A $\beta$  plaques was quantified manually by counting the number of A $\beta$  plaques with clustered microglia. As positive plaque with microglia clusters we defined the abundance of 2–5 microglia cells surrounded by a small halo of tissue with low or without presence of microglia processes. In classical AD, such clusters or nodules are associated with neuritic or core plaques, but rarely seen in diffuse plaques.

In fluorescence staining where two primary antibodies came from the same species (rabbit), a triple staining was performed using extensive heat-induced epitope retrieval. The paraffin-embedded tissue was deparaffinized, and slices were steamed for 45 min in EDTA pH 9.0. Non-specific protein binding was blocked by incubation with diluent. The first primary Antibody (P2ry12 or Tmem119) was applied over night at 4°C and on the following day reapplied at room temperature for 1 hr. Consequently, we incubated sections with biotinylated anti-rabbit antibody and then with avidin-coupled peroxidase, which catalyzed signal amplification with tyramide. Antigen retrieval was repeated by steaming with EDTA pH 9.0 for 30 min, which abolishes antibody reactivity from the previous round but leaves the amplified avidin binding intact, thus preserving the localized binding of Cy2 labeled streptavidin. In a next step two additional primary antibodies were simultaneously applied overnight at 4°C (Iba-1+SMI31 or A $\beta$ ; Tmem119+SMI31 or A $\beta$ ) and reapplied the next day for one hour at room temperature. Secondary antibodies anti-rabbit Cy5 (Iba-1/Tmem119) and anti-mouse Cy3 (Smi31/ Amyloid  $\beta$ ) used for visualizing the immunohistochemical reaction. Covering with slips was done by mounting with Gallate Geltol for 5 min.

For Fluoro-Jade C staining, frozen cut tissue sections were first immersed in a basic alcohol solution consisting of 1% sodium hydroxide in 80% ethanol for 5 min, then rinsed for 2 min in 70% ethanol, for 2 min in distilled water and finally, incubated in 0.06% potassium permanganate solution for 2 min. Slides were then transferred for 10 min to a 0.0001% solution of Fluoro-Jade C (Histo-Chem Inc; Jefferson, AR) dissolved in 0.1% acetic acid vehicle. Slides were then rinsed three times in distilled water for 1 min, cleared in xylene and coverslipped with DPX (Sigma).

### Analysis of P2RY12 and Dystrophic Axons in AD Brains

Independent patient cohort Quantitative evaluation for P2RY12 and dystrophic axons was performed by manual counting. Plaques were identified using the anti-Amyloid $\beta$  antibody, Clone W02 (Millipore). Following immunohistochemistry on respective serial sections the previously defined regions of interest (ROI) were manually outlined. In the individual cases three different ROIs were quantified by overlaying a morphometric grid ( $0.27 \text{ mm}^2$ ) placed within the ocular lens: two fields in areas with the highest density of P2RY12 reactive microglia, two fields in areas of intermediate density and two fields in areas of the lowest density within the respective case and lesion.

### Induction of EAE

For the PLP-induced EAE, SJL/J female mice (6–8 weeks old) were immunized subcutaneously (s.c.) with 200  $\mu\text{g}$  of PLP139–151 peptide in a 0.2 mL emulsion comprised of equal volumes of phosphate-buffered saline (PBS) solution. For the MOG-induced EAE, female mice (6–8 weeks) were injected s.c. in both flanks with 100  $\mu\text{g}$  myelin oligodendrocyte glycoprotein (MOG) 35–55 peptide dissolved in PBS. For both models, the solutions were emulsified in an equal volume of CFA (Difco) containing killed *Mycobacterium tuberculosis* strain H37RA at a final concentration of 5 mg ml $^{-1}$  *Mycobacterium tuberculosis* H37Ra and injected twice i.p. with 200 ng pertussis toxin (List Biological Laboratories, Campbell, CA) administered on the day of immunization and 48 hr later. Clinical assessment of EAE was performed daily after disease induction according to the following criteria: 0, no signs of disease; 1, loss of tone in the tail; 2, hind limb paresis; 3, hind limb paralysis; 4, tetraplegia; 5, moribund, during the duration of the acute phase (15 d), or only during the progressive or chronic phase (days 30–50). Microglia from these mice were sorted at the scores (i.e., 0, 1, 2, 3) indicated in Figures 1A and 1B and Table S1.

### Isolation of Primary Neurons

Primary neurons were prepared from embryos at age E18.5. Cerebral hemispheres were isolated and freed from meninges. Tissues were digested with 0.25% trypsin in HBSS for 15 min at 37°C, and triturated with fire-polished glass pipettes to obtain single cell preparation. Cell suspension was filtered through a 70 and a 40 µm cell strainer, and cells were collected at 1,000 g for 5 min. Cell density was then determined using a hemocytometer, and cells were seeded at different densities according to the experimental design and need. We used DMEM supplemented with 10% FBS for the initial plating, and the medium was changed to Neurobasal supplemented with 1 × B27 (Invitrogen) 3 h later. Half medium was changed every 3 days.

### Induction of Apoptosis and Labeling of Neurons

To induce apoptosis, neurons were carefully detached from the plate surface by repeated washes with PBS. Neurons were irradiated with UV light (302 nm) with an intensity of 6 × 15 W for 15 min. From now on, neurons were kept on ice. Cells were harvested by centrifugation and the pellet processed for downstream applications. The labeling dye (1mg) was resuspended in 100 µL special anhydrous DMSO (Thermo Fisher Scientific) and immediately used. Alternatively, dissolved dye was quickly aliquoted at 5 µL and stored at –80°C until use. Neurons were carefully resuspended in 1 mL of PBS and incubated in darkness for 15 min at 37°C with 2 µL of the dissolved labeling dye (Alexa488 5-SDP Ester or Alexa405 NHS Ester, Life Technologies/Thermo Fisher Scientific). To block and capture residual dye, cells were diluted with PBS, harvested by centrifugation, resuspended in 1 mL FBS and washed twice with PBS. Total apoptotic cell number was determined using Trypan Blue staining. Neurons were resuspended at a density of approximately 100,000 cells per 4 µL for stereotactic injection.

### Induction of Necrosis in Neurons

To induce necrosis, plated neurons were irradiated with UV light for 15 min and then placed back in the incubator for 24 hr. Neurons were labeled with Alexa488 5-SDP Ester (Life Technologies). To distinguish between apoptotic and necrotic cells, dying neurons were incubated with Annexin V (Biolegend) and 7-AAD (Biolegend, 5 µg ml<sup>-1</sup>) for 5 min before flow cytometry analysis.

### Stereotactic Injections

Mice were anesthetized by i.p injection of a mixture of Ketamine (100 mg kg<sup>-1</sup>), Xylazine (10 mg kg<sup>-1</sup>) and Acepromazine (3 mg kg<sup>-1</sup>). 2 µL of compound (which could be labeled as dNs, recombinant mouse APOE [0.5 mg mL<sup>-1</sup> My Biosource], bacterial LPS [Sigma], Zymosan [Life Technologies], or *E. coli* [Life Technologies]) or saline solution were each distributed into the hippocampus and cortex bilaterally (Y: ± 1.5mm; X: –2mm; Z: –2mm and –1mm) using stereotaxic equipment (Harvard Apparatus). After recovery from surgery, animals were returned to their home cages. Post-surgery (16 hr or 3 days), mice were euthanized by CO<sub>2</sub> inhalation and perfused for subsequent experiments.

### Intrahippocampal Injection of Kainic Acid

Mice were injected into the dorsal hippocampus of both hemispheres with Kainic acid dissolved in saline (0.2 µg in 50 nl) using a microsyringe (Hamilton, Reno, Nevada) with a 26-gauge needle and the stereotaxic coordinates from bregma: anteroposterior (AP), -1.8 mm; mediolateral (ML), 1.6 mm; dorsoventral (DV), -1.8 mm. Control animals received 0.9% NaCl under the same surgical conditions. After 48 hr, mice were euthanized by CO<sub>2</sub> inhalation and perfused for subsequent experiments.

### Facial Nerve Axotomy

Unilateral facial nerve transection at the stylomastoid foramen was performed in WT, *ApoE*<sup>–/–</sup>, *Trem2*<sup>–/–</sup>, and *Cx3cr1*<sup>CreERT2</sup>.*ApoE*<sup>f/f</sup> and *Cx3cr1*<sup>wt</sup>.*ApoE*<sup>f/f</sup> (control) mice (n = 4–5/group). Successful nerve injury indicated by ipsilateral whisker paresis was assessed upon recovery from mild anesthesia by isoflurane. All mice were sacrificed at 7 days post-facial nerve axotomy. Immunohistochemical staining for NeuN (clone A60, Millipore, 2 µg ml<sup>-1</sup>) and P2ry12 (polyclonal, 0.4 µg ml<sup>-1</sup>) and analyses were performed on 30 µm floating sections as described in previous section. For quantification of NeuN<sup>+</sup> neurons, only cells within the facial motor nucleus with fully visible cell bodies and visible cytoplasm were included.

### Mouse Microglia Isolation and Sorting

Microglia isolation was performed according to our previously described protocol (Butovsky et al., 2014). Briefly, mice were transcardially perfused with ice-cold Hanks' Balanced Salt Solution (HBSS), spinal cords and brains separately dissected. For sample post-stereotaxic injection, tissue around the site of injection was collected corresponding to the following measurements 3x4x4 mm/hemisphere and a mass in average of ~90 mg. From this tissue, ~1,000 phagocytic cells and 20,000 non-phagocytic cells were sorted in average from the same site of injection for Nanostring, RNaseq and qPCR analyses. Single cell suspensions were prepared and centrifuged over a 37%/70% discontinuous Percoll gradient (GE Healthcare), mononuclear cells were isolated from the interface. In order to distinguish resident microglia from recruited myeloid cells, we used a monoclonal antibody that recognizes FCRLS, which is expressed on microglia, but not on infiltrating myeloid cells (Butovsky et al., 2014). Isolated cells were stained with anti-FCRLS [clone 4G11, 3 µg ml<sup>-1</sup>, validated in ref.], followed by secondary detection with goat anti-rat IgG conjugated to APC [clone Poly4054, Biolegend, 0.7 µg ml<sup>-1</sup>, validated in reference (Butovsky et al., 2014)] and then CD11b-PeCy7 [clone M1/70, BD Biosciences, 2 µg ml<sup>-1</sup>, validated in reference (Butovsky et al., 2014)] antibody to specifically sort resident microglia. Phagocytic versus non-phagocytic microglia were further sorted from the FCRLS<sup>+</sup>CD11b<sup>+</sup>-population by detection of Alexa488

fluorescence. FCRLS<sup>+</sup>Clec7a<sup>+</sup>, FCRLS<sup>+</sup>Clec7a<sup>Int</sup> and FCRLS<sup>+</sup>Clec7a<sup>-</sup> cells were sorted using mClec7a (clone R1-8g7, Invivogene, 1:10) and FITC goat-anti-rat (BioLegend #405404, 1:100).

### Isolation of Spleenic CD11b<sup>+</sup>Ly6C<sup>+</sup> Monocytes

Spleen was dissected and homogenized using a cell strainer (70 µm). After centrifugation, the cell pellet was resuspended in ACK lysis buffer to remove red blood cells. Splenocytes were incubated with anti-CD11b magnetic beads (1:10, Miltenyi Biotec) for 15 min on ice. CD11b<sup>+</sup> cells were collected after magnetic separation. Unspecific antigen binding sites were blocked using Fc Receptor blocking anti-CD16/32 antibodies (BD Biosciences, 5 µg ml<sup>-1</sup>) and cells were stained using anti-Ly6C-FITC and anti-CD11b-PeCy7 (BD Biosciences, 5 µg ml<sup>-1</sup>) and sorted accordingly.

### Mass Spectrometry Analysis

Single LC-MS/MS experiment was performed on a LTQ Orbitrap Velos (Thermo Fischer) equipped with Waters (Milford, MA) NanoAcuity HPLC pump. Peptides were separated onto a 100 µm inner diameter microcapillary trapping column packed first with approximately 5 cm of C18 ReproSil resin (5 µm, 100 Å, Dr. Maisch GmbH, Germany) followed by ~20 cm of ReproSil resin (1.8 µm, 200 Å, Dr. Maisch GmbH, Germany). Separation was achieved through applying a gradient from 5%–27% ACN in 0.1% formic acid over 180 or 600 min at 100 nL min<sup>-1</sup>. Electrospray ionization was enabled through applying a voltage of 1.8 kV using a home-made electrode junction at the end of the microcapillary column and sprayed from fused silica pico tips (New Objective, MA). The LTQ Orbitrap Velos was operated in data-dependent mode for the mass spectrometry methods. The mass spectrometry survey scan was performed in the Orbitrap in the range of 395 –1,800 m/z at a resolution of  $6 \times 10^4$ , followed by the selection of the twenty most intense ions (TOP20) for CID-MS2 fragmentation in the Ion trap using a precursor isolation width window of 2 m/z, AGC setting of 1,000, and a maximum ion accumulation of 200 ms. Singly charged ion species were not subjected to CID fragmentation. Normalized collision energy was set to 35 V and an activation time of 10 ms. Ions in a 10 ppm m/z window around ions selected for MS2 were excluded from further selection for fragmentation for 60 s. The same TOP20 ions were subjected to HCD MS2 event in Orbitrap part of the instrument. The fragment ion isolation width was set to 0.7 m/z, AGC was set to 10,000, the maximum ion time was 200 ms, normalized collision energy was set to 27V and an activation time of 1 ms for each HCD MS2 scan. Raw data were submitted for analysis in Proteome Discoverer 2.2.0.386 (Thermo Scientific) software. Assignment of MS/MS spectra was performed using the Sequest HT algorithm by searching the data against a protein sequence database including all entries from the Mouse Uniprot database (SwissProt 16,768 2016) and other known contaminants such as human keratins and common lab contaminants. Sequest HT searches were performed using a 20 ppm precursor ion tolerance and requiring each peptides N-/C termini to adhere with Trypsin protease specificity, while allowing up to two missed cleavages. 6-plex TMT tags on peptide N termini and lysine residues (+229.162932 Da) was set as static modifications while methionine oxidation (+15.99492 Da) was set as variable modification. A MS2 spectra assignment false discovery rate (FDR) of 1% on protein level was achieved by applying the target-decoy database search. Filtering was performed using a Percolator (64bit version). For quantification, a 0.02 m/z window centered on the theoretical m/z value of each the six reporter ions and the intensity of the signal closest to the theoretical m/z value was recorded. Reporter ion intensities were exported in result file of Proteome Discoverer 2.2 search engine as an excel tables. The total signal intensity across all peptides quantified was summed for each TMT channel, and all intensity values were normalized to account for potentially uneven TMT labeling and/or sample-handling variance for each labeled channel.

### RNA Isolation and NanoString RNA Counting

Total RNA was extracted using mirVana miRNA isolation kit (Ambion) according to the manufacturer's protocol. NanoString nCounter technology (<http://www.nanostring.com/>) allows expression analysis of multiple genes from a single sample (Butovsky et al., 2014). We performed nCounter multiplexed target profiling of 400 to 542 microglial transcripts (MG400 and MG550, see MG custom-chip design). 100 ng of total RNA per sample were used in all described nCounter analyses according to the manufacturer's suggested protocol (Butovsky et al., 2014).

### Quantitative Real-Time PCR

For conventional quantitative reverse transcription polymerase chain reaction (qRT-PCR), total RNA (30 ng) with specific mRNA probes and 3 ng of RNA with specific miRNA probes (Applied Biosystems) were used after reverse transcription reaction according to the manufacturer (high-capacity cDNA Reverse Transcription Kit; Applied Biosystems). All mRNA/miRNA amplifications were performed with commercially available FAM-labeled Taqman probes (Applied Biosystems/Thermo Fisher Scientific). mRNA or miRNAs levels were normalized relative to GAPDH or U6, respectively. Real-time PCR reaction was performed using Vii7 (Applied Biosystems). All qRT-PCRs were performed in duplicate, and the data are presented as relative expression compared to GAPDH or U6 as mean ± s.e.m.

### Mouse MG550 Chip Design

The MG550 NanoString chip was designed using the quantitative NanoString nCounter platform. Selection of genes is based on analyses that identified genes and proteins which are specifically or highly expressed in adult mouse microglia (Butovsky et al., 2014) plus 40 inflammation-related genes which were significantly affected in EAE, APP-PS1 and SOD1 mice. Two other versions were done after MG400 (Butovsky et al., 2014). MG468 contains additional 48 inflammation- and phagocytosis-related genes (Butovsky

et al., 2015). Using this signature, we generated a new version of NanoString-based microglia chip termed MG550 that encompasses 400 unique and enriched microglial genes we have identified previously (Butovsky et al., 2014) and additional 150 inflammation-, inflammasome- and phagocytosis-related genes.

### NanoString Data Analysis

NanoString data were normalized and analyzed using nSolver software. RNA ncounts were normalized using the geometric mean of 6 housekeeping genes (HKGs): *Cltc*, *Gapdh*, *Gusb*, *Hprt*, *Pgk1*, and *Tubb5*. A cutoff was introduced at the value of the highest negative control present on the chip. Fold changes were calculated using the average of each group. For each experiment, the fold changes were calculated comparing the experimental group to their appropriate controls.

### RNA Sequencing

1,000 FACS-sorted FCRLS<sup>+</sup> microglia cells were lysed in TCL buffer. Smart-Seq2 libraries were prepared by the Broad Technology Labs and sequenced by the Broad Genomics Platform. cDNA libraries were generated from sorted cells using the Smart-seq2 protocol (Picelli et al., 2013). RNA sequencing was performed using Illumina NextSeq500 using a High Output v2 kit to generate 2 × 25 bp reads. RNA-Sequencing data was pooled from 3 separate experiments. Transcripts were quantified by the BTL computational pipeline using Cuffquant version 2.2.1 (Trapnell et al., 2012). Raw counts were normalized using TMM normalization and then log2-transformed. Batch effects were corrected using removeBatchEffect from the R package limma (v. 3.28.21).

### In Vitro Suppression Assay

Spleens of C57BL/6J mice were gently dissociated into single-cell suspensions, and red blood cells were removed using Ammonium-Chloride-Potassium (ACK) lysis buffer (GIBCO). Splenocytes were labeled with 5(6)-Carboxyfluorescein N-hydroxysuccinimidyl ester (CFSE, Molecular probes – Invitrogen, 5 µmol l<sup>-1</sup>) at 37°C followed by staining with anti-CD3 mAb (clone 145-2C11, Biolegend, 2 µg ml<sup>-1</sup>) for 30 min on ice. Responder CFSE<sup>+</sup> CD3<sup>+</sup> T cells were sorted using FACS Aria II (BD Biosciences) with a purity > 98%. T cells were stimulated with mouse T cell-activator CD3 and CD28 magnetic beads (Dynabeads-GIBCO). Stimulated CFSE<sup>+</sup> CD3<sup>+</sup> T cells were co-cultured in round bottom 96-well plates with FCRLS<sup>+</sup> spinal cord microglia for 72 hr at 37°C in a 5% CO<sub>2</sub> incubator. T cell-to-microglia ratio was 4:1 in a final volume of 200 µL per well in DMEM media supplemented with 10% Fetal Bovine Serum (FBS), 1% Penicillin-Streptomycin (PS, 10,000 U ml<sup>-1</sup>), L-Glutamine 2 mmol l<sup>-1</sup>, sodium pyruvate 1 mmol l<sup>-1</sup>, non-essential amino acids 0.1 mmol l<sup>-1</sup>, HEPES 5 mmol l<sup>-1</sup> and 2-Mercaptoethanol 0.05 mmol l<sup>-1</sup>. T cell proliferation was measured by flow cytometric analysis by CFSE dilution on CD3<sup>+</sup> T cells. Soluble recombinant ApoE (rApoe) was added into the media at 100 ng ml<sup>-1</sup>.

### Heatmaps

Heatmaps and clustering were generated in R (version 3.2.0) using heatmap.2 from the gplots package and the prcomp from the stats package. For clustering, the z-scores were calculated using the mean expression of biological replicates per disease stage/condition and then subsequently clustered using K-means. A scree plot was used to assess the number of clusters.

### Circos Plot

The custom-made microglia transcriptional signatures (Figure 3I) were generated by retrieving genes upregulated at least 1.5 fold and p value less than 0.01 (Student t test) in disease conditions from previously identified microglia transcriptomes from mouse models of neuropathic pain (GSE60670), chronic pain (GSE71133), Rett syndrome (*Mecp2*<sup>-/-</sup>) (GSE66211), lipid disorder (*Mfp2*<sup>-/-</sup>) (GSE66420), ALS (SOD1) (GSE43366), AD (5xFAD) (GSE65067), brain irradiation (GSE55968), and aging (GSE62420). All custom signatures were derived from publicly available transcriptomes downloaded from Gene Expression Omnibus (GEO). A GSEA algorithm was applied to identify the enrichment of phagocytic microglia signaling pathways in the microglia transcriptomes in various diseases conditions. This includes Aging, *Mfp2*-deficiency, Alzheimer's disease, ALS, neuropathic pain, chronic pain, and *Mecp2*-deficiency. GSEA assesses whether the expression of a previously defined group of related genes is enriched in one biological state. Statistical significance of GSEA results was assessed using 1,000 sample permutations. A nominal P value less than 0.001 was used to determine pairwise transcriptome connectivity. A Circos graph was generated using Circos package 0.68.12.

TREM2 pathway analysis in MGnD microglia. A GSEA algorithm was used to identify genes that are differentially expressed in microglia transcriptomes from lipid disorder (*Mfp2*<sup>-/-</sup>) (GSE66420), ALS (SOD1) (GSE43366), AD (5xFAD) (GSE465067), and aging (GSE62420), as compared with their control counterparts. High-scoring differentially expressed 'leading-edge' genes were selected on the basis of their presence in the TREM2-responsive gene signature 5xFAD:*Trem2*<sup>-/-</sup> and SOD1:*Trem2*<sup>-/-</sup> mice. The statistics were determined using Euclidean distance.

### Ingenuity Pathway Analysis

Data were analyzed using Ingenuity software (Ingenuity Systems, <http://www.ingenuity.com>). Differentially expressed genes (with corresponding n-fold changes and p values) were incorporated in canonical pathways and bio-functions and were used for generating biological networks as described previously (Butovsky et al., 2014). Briefly, uploaded dataset for analysis was filtered using the following cutoff definitions: fivefold change, p < 0.01.

## QUANTIFICATION AND STATISTICAL ANALYSIS

Statistical analysis was done using GraphPad Prism 7 software. Data distribution was assumed to be normal, but this was not formally tested. Data are presented as mean  $\pm$  s.e.m and 2-tailed Student's t tests (unpaired) or ANOVA multiple comparison tests were used to assess statistical significance. Data collection and analysis were blindly performed. Data for each experiment were collected and processed randomly and animals were assigned to various experimental groups randomly as well. All n and P values and statistical tests are indicated in figure legends. Volcano plots were generated using Multiplot studio software. Heatmaps were generated using MEV and R-software.

## DATA AND SOFTWARE AVAILABILITY

The accession number for the RNAseq and Nanostring gene sequence data reported in this paper is Gene Expression Omnibus (GEO): GSE101689. The accession number for the protein data reported in this paper is PeptideAtlas: PASS01081.